LA-UR-16-29622

Proton and Ion Linear Accelerators

9. Emittance Growth, Halo Formation, and Beam Loss

Yuri Batygin
Los Alamos National Laboratory

U.S. Particle Accelerator School

July 15 - July 26, 2024

Sources of Beam Loss

1. Misalignments and lattice errors
2. Transverse-longitudinal coupling in RF field
3. Nonlinearities of focusing and accelerating elements
4. Non-linear space-charge forces of the beam
5. Mismatch of the beam with accelerator structure
6. Beam envelope resonances, particle–core resonances, beam core-core resonances
7. Variation and instabilities of accelerating and focusing field
8. Redistribution of beam distribution in 6D phase space
9. Beam energy tails from un-captured particles
10. Excitation of higher-order RF modes
11. Particles interaction with residual gas, intra-beam stripping, field stripping, photon stripping
12. Dark currents (un-chopped beam, RF transients)
13. Black body radiation

Requirements on Hands-On Maintenance of Accelerator

Beam loss results in radiation activation of the accelerator, which can be distinguished as prompt and residual. Prompt activation requires shielding of the accelerator tunnel. Residual activation imposes limits on maintenance on the accelerator after the termination of operation.

Level of Residual Activation and Type of Maintenance

Level of Activation	Type of Maintenance
< 10 mrem/hr	Unconstrained "hands-on" maintenance
10 mrem/hr – 100 mrem/hr	Hands-on maintenance, limited access time
100 mrem/hr – 10 rem/hr	Hands-on maintenance, strictly controlled, very limited access time
>10 rem/hr	Remote maintenance required

Residual Activation of Accelerator

$$\text{Dose rate [mrem/h]} = \frac{0.33(W[\text{MeV}] - 9)^{1.8}}{W[\text{MeV}]}$$

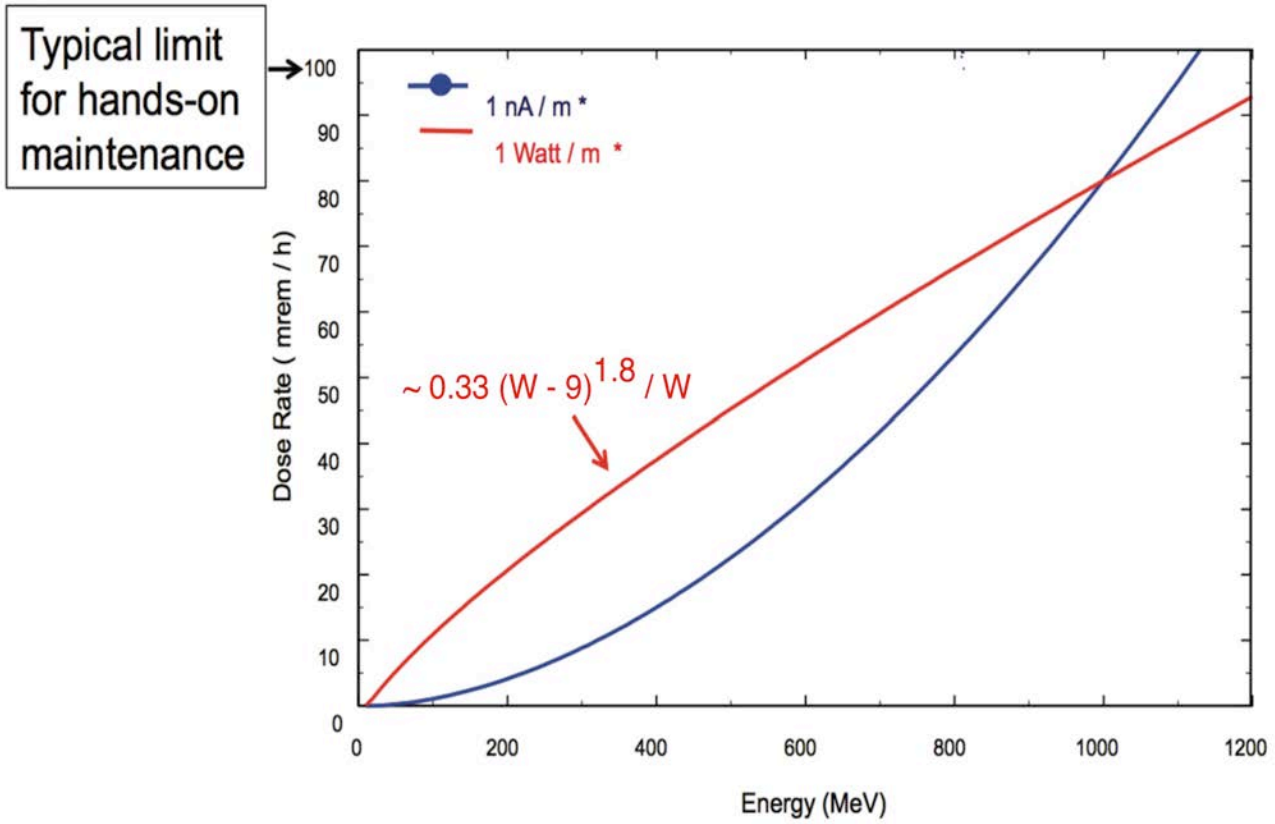

Residual activation as a function of beam energy (R. Handekopf, 1999; J. Galambos, 2021).

Dose rate is measured at 30 cm from the accelerator after 4 hours of accelerator cooldown following 100 days of steady-state accelerator operation.

Allowable Beam Loss

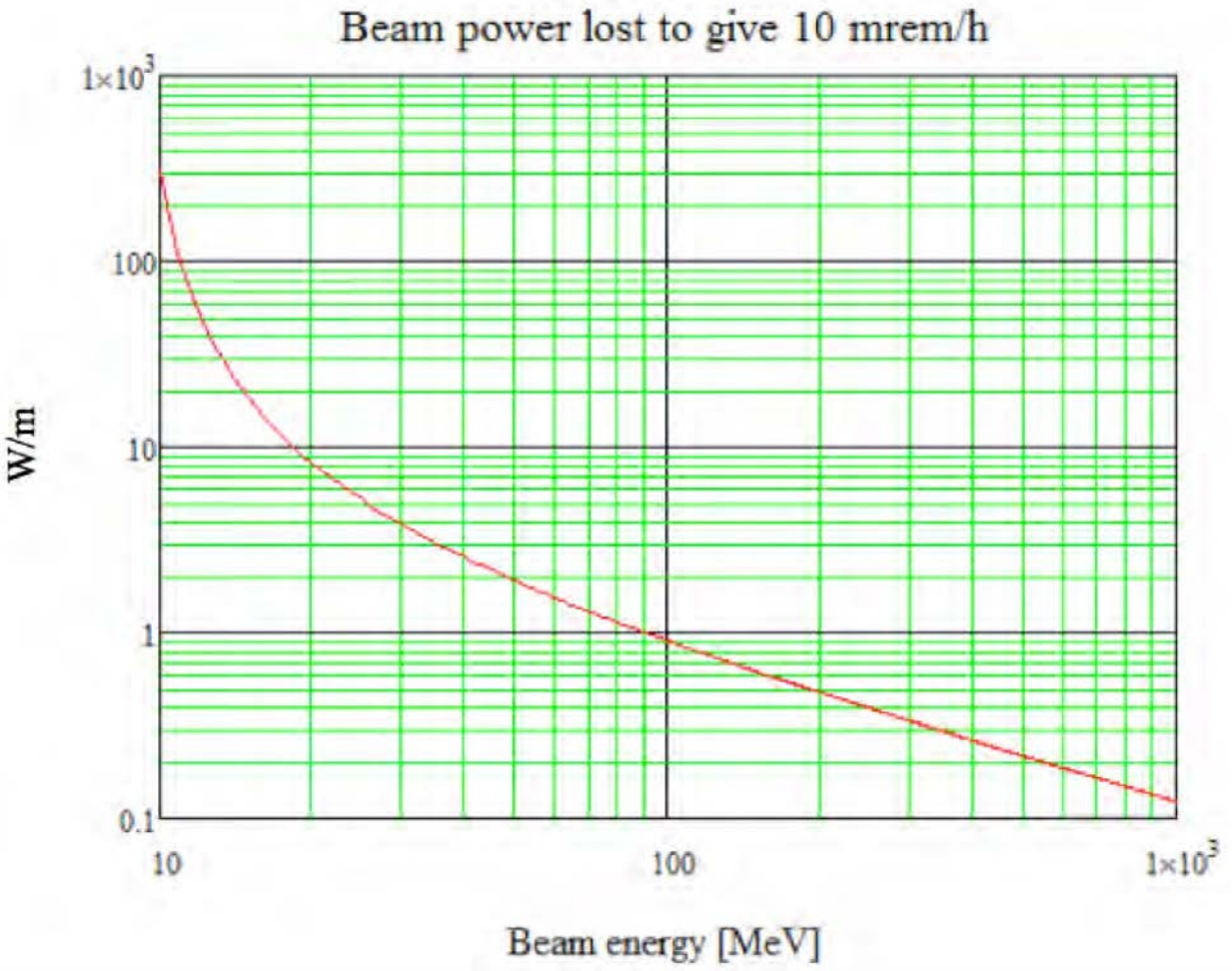

In high-energy linac, required beam losses: is less than 1 W/m.

For beam power 1 MW beam losses should be less than 10^{-6}/m.

Allowable beam power loss versus beam energy to produce an activation of 0.1 mSv/h (10 mrem/h) at 30 cm for the case of copper, after 4 h cool down (M. Plum, CERN-2016-002).

Beam Loss Monitors

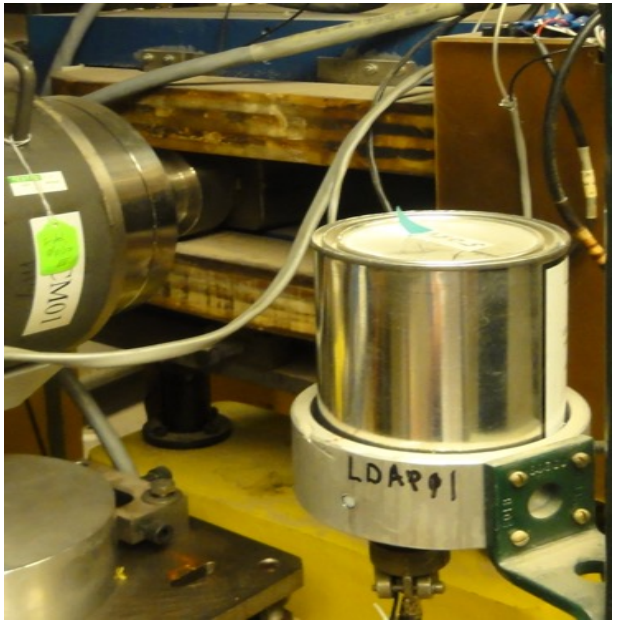

Activation Protection (AP) scintillation detector.

Ion Chamber (IR) and Gamma Detector (GD).

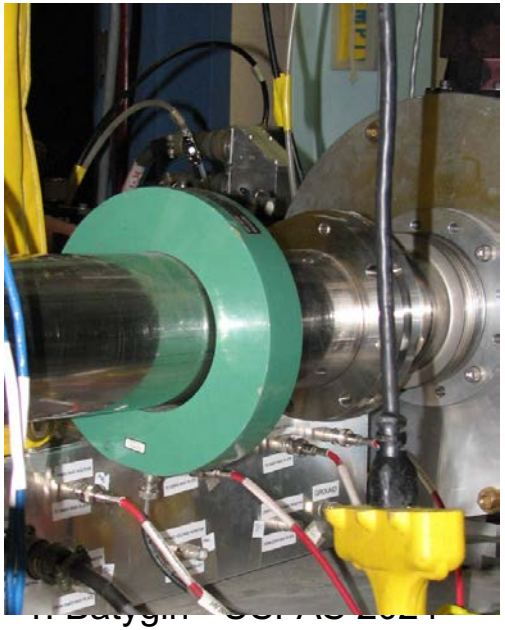

Hardware Transmission Monitors (HWTM) measures the beam current losses between current monitors and limit beam current to a value at one current monitor.

Beam Losses in LANL Linear Accelerator

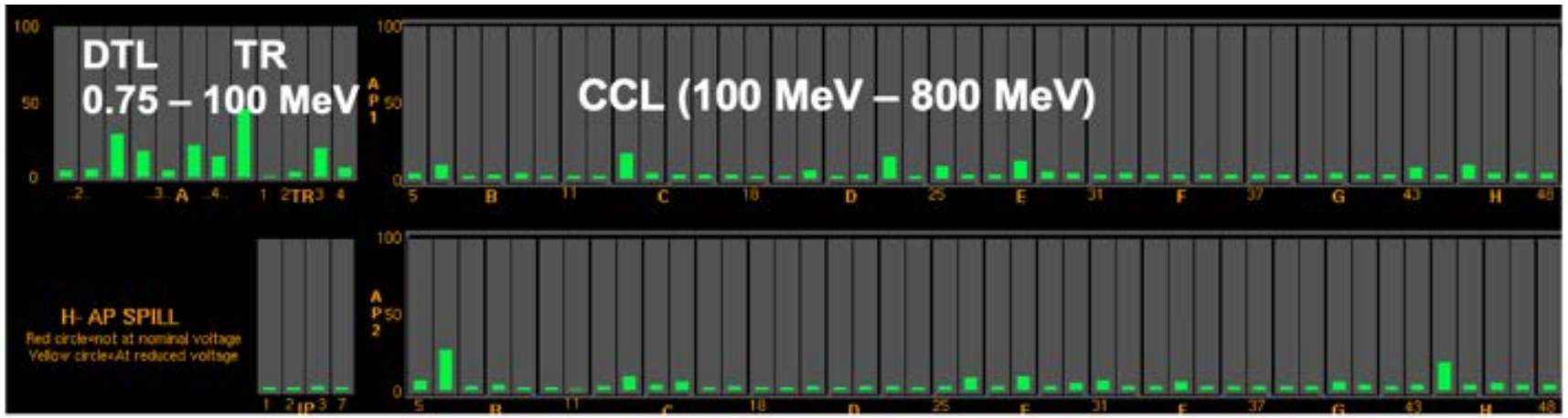

LANL linac loss monitors (Activation Protection devices): liquid scintillator and photomultiplier tube, calibrated against 100 nA point spill. Average beam losses are 0.1 – 0.2 W/m.

Year	Pulse Rate (Hz)	Summed Loss Monitor Reading (A.U.)
2018	120/60	180
2017	120	150
2016	120	190
2015	120	135
2014	60	211
2013	60	190

LANL 800 MeV Beam Loss

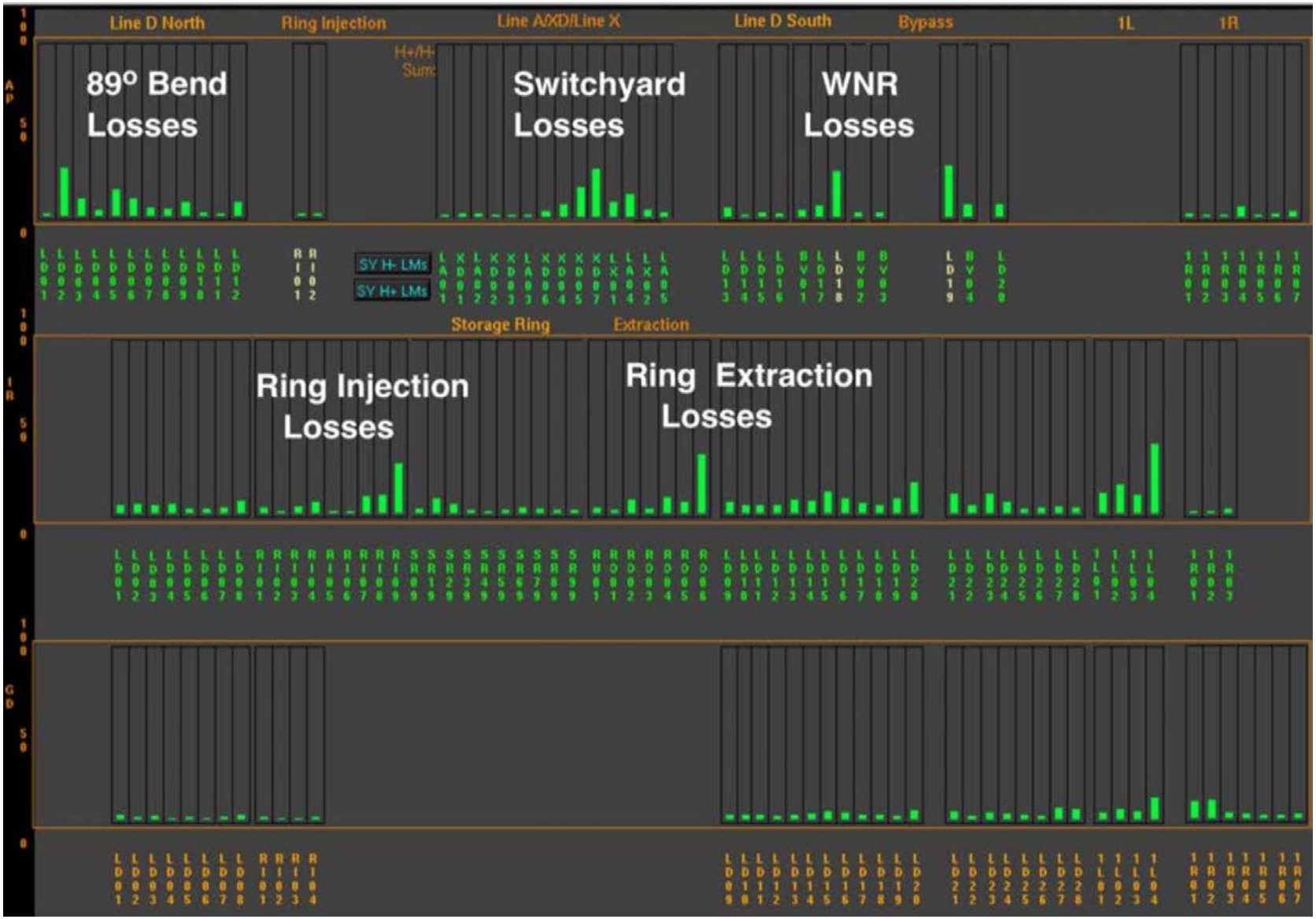

Vibrating Wire Sensor as a Halo Monitor

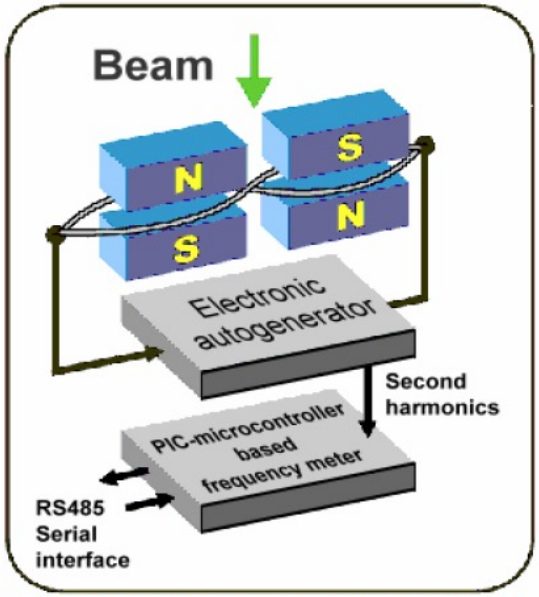

Vibrating wire scanner test in lab [Arutunian et. al., PAC (March 29 - April 2, 1999, New York City)]

The operating principle of vibrating wire sensors is measurement of the change in the frequency of a vibrating wire, which is stretched on a support, depending on the physical parameters of the wire and the environment in

By use of a simple positive feedback circuit, the magnetic system excites the second harmonic of the wire's natural oscillation frequency while keeping the middle of the wire exposed for detection of beam heating.

The interaction of the beam with the wire mainly causes heating of the wire due to the energy loss of the particles

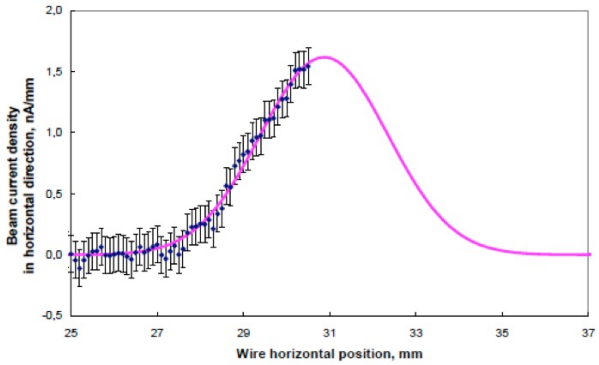

Scan of the electron beam at the Injector of Yerevan Synchrotron with an average current of about 10 nA (after collimation) and an electron energy of 50 MeV

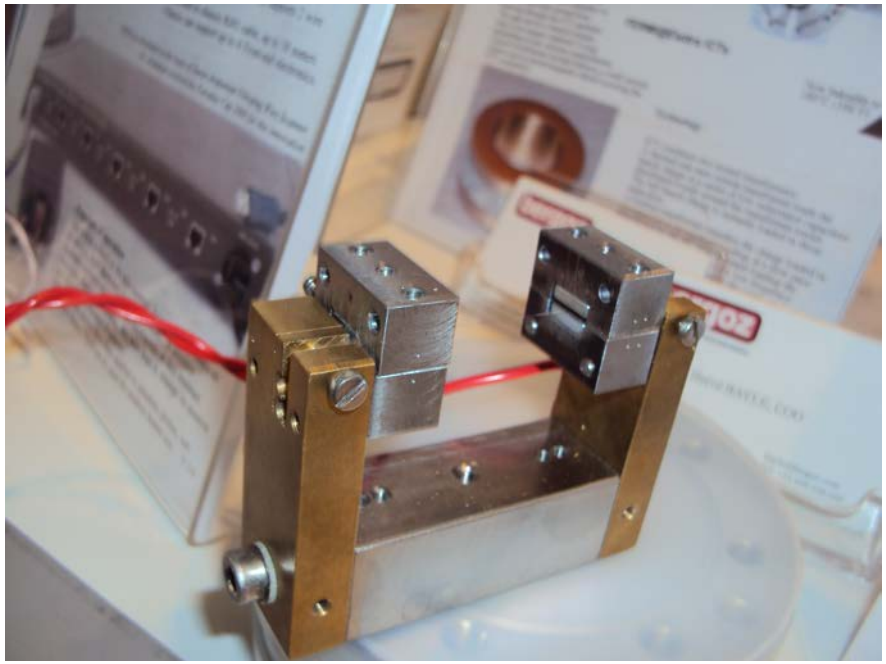

Linac Beam Distribution in Phase Space

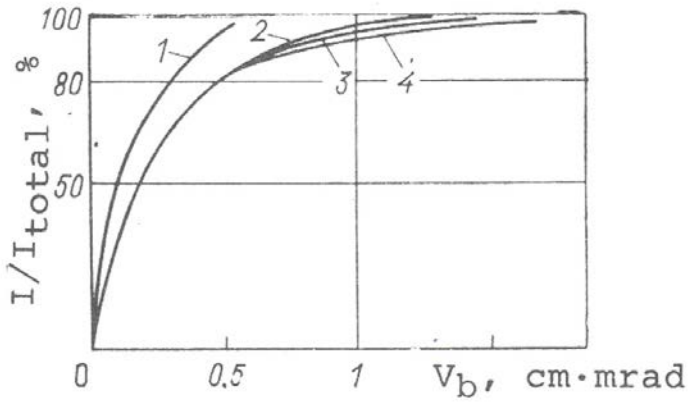

Fig. 4.8 The distribution of the current in the phase space of the beam at different points in the CERN proton accelerator-injector. 1--0.5 MeV, 115 mA; 2--10 MeV; 3--30 MeV; 4--50 MeV, 58 mA.

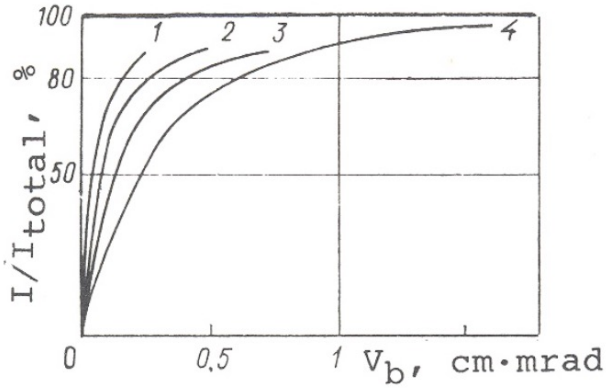

Fig. 4.9 The distribution of the current in the phase space of the beam in the FNAL proton accelerator-injector. 1--0.75 MeV, 150 ma; 2--10 MeV; 3 and 4--200 MeV, 78 mA.

Beam Distribution as a Function of Beam Intensity

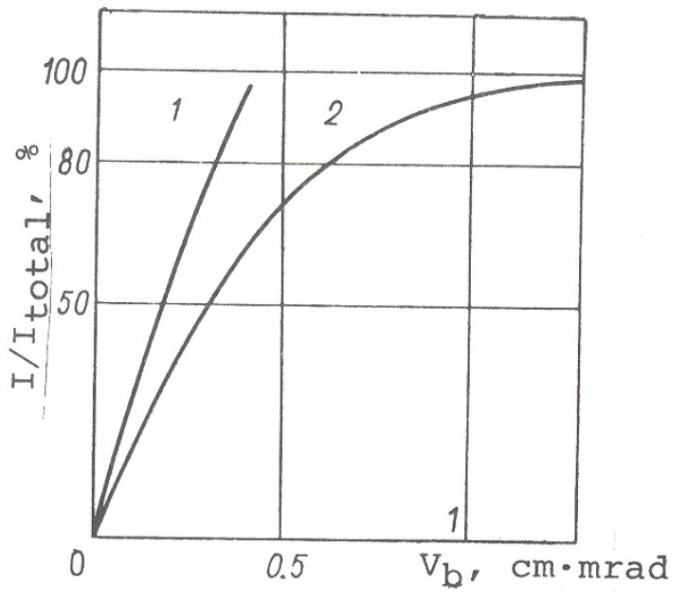

Fig. 4.10 The distribution of the current in the phase space of the beam at the entrance and exit of the ITEP proton accelerator-injector. 1--0.7 MeV, 470-600 mA; 2--25 MeV, 160-200 mA.

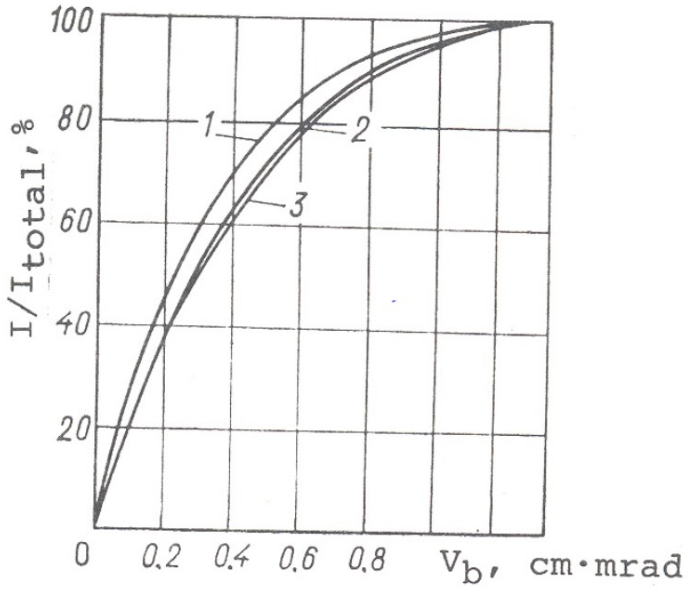

Fig. 4.11 The distribution of the current in the phase space of the beam at the exit of the ITEP accelerator-injector for different values of the total current of the accelerated beam. 1--60-100 mA; 2--100-160 mA; 3--160-200 mA.

Empirical experimental dependence of beam emittance growth in RF linac versus beam current *I* (0.6< n <1.0)

$$\varepsilon_{out} = \sqrt{\varepsilon_{in}^2 + kI^n}$$

Beam Halo

1. Beam halo - a collection of particles which lies outside of beam core and typically contain small fraction of the beam (less than 1%).
2. Beam halo is a main source of beam losses which results in radio-activation and degradation of accelerator components.
3. Modern accelerator projects using high-intensity beams with final energies of 1-1.5 GeV and peak beam currents of 30-100 mA require keeping the beam losses at the level of 10^{-7}/m (less than 1 W/m) to avoid activation of the accelerator and allowing hands-on maintenance over long operating periods.
4. Collimation of beam halo cannot prevent beam losses completely, because the halo of a mismatched beam re-develops in phase space after a certain distance following collimation.

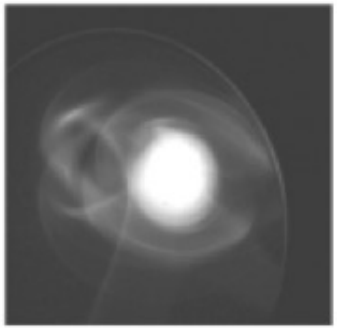

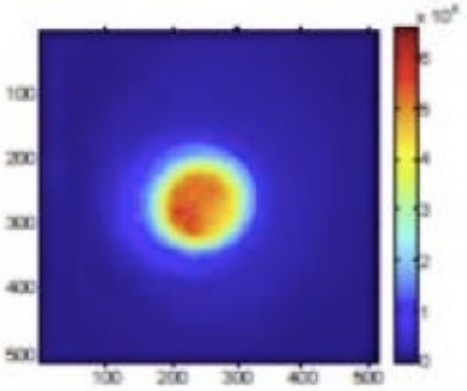

Beam halo monitoring at Liverpool University

http://liv.ac.uk/quasar/research/beam-instrumentation/beam-halo-studies/

Beam Halo (cont.)

One of the ways to reduce beam halo at certain distance is beam scrapping at low energy. It results in reduction of beam loss in DTL and at certain points at High-Energy Beam Transport. However, collimation of a beam halo cannot prevent beam losses at longer distance, because the halo re-develops after a certain distance following collimation. Experiments performed at SNS (Oak Ridge Nat Lab) show that when the beam reaches the final energy of 1 GeV, there is a very little measurable difference in the beam halo with or without MEBT scrapping.

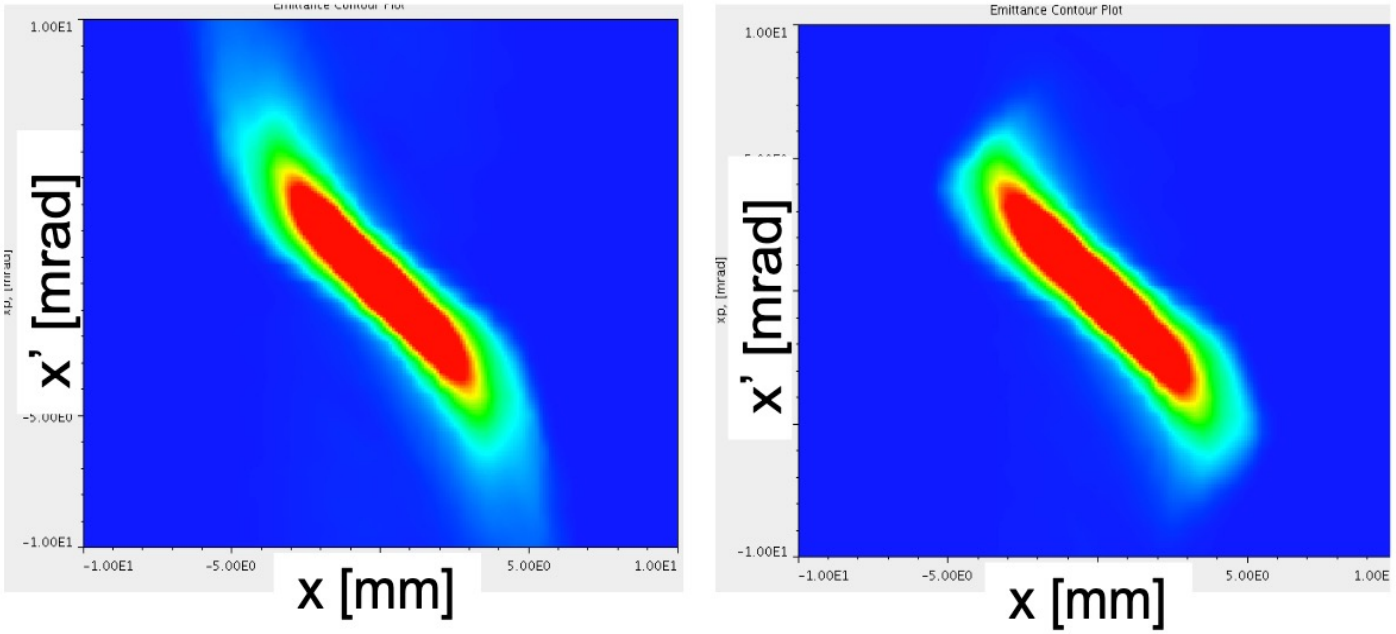

Collimation of beam halo at SNS 2.5-MeV beam scrapper: (a) before collimation, (b) after collimation [Zhukov et al, LINAC2010].

Beam Halo (cont.)

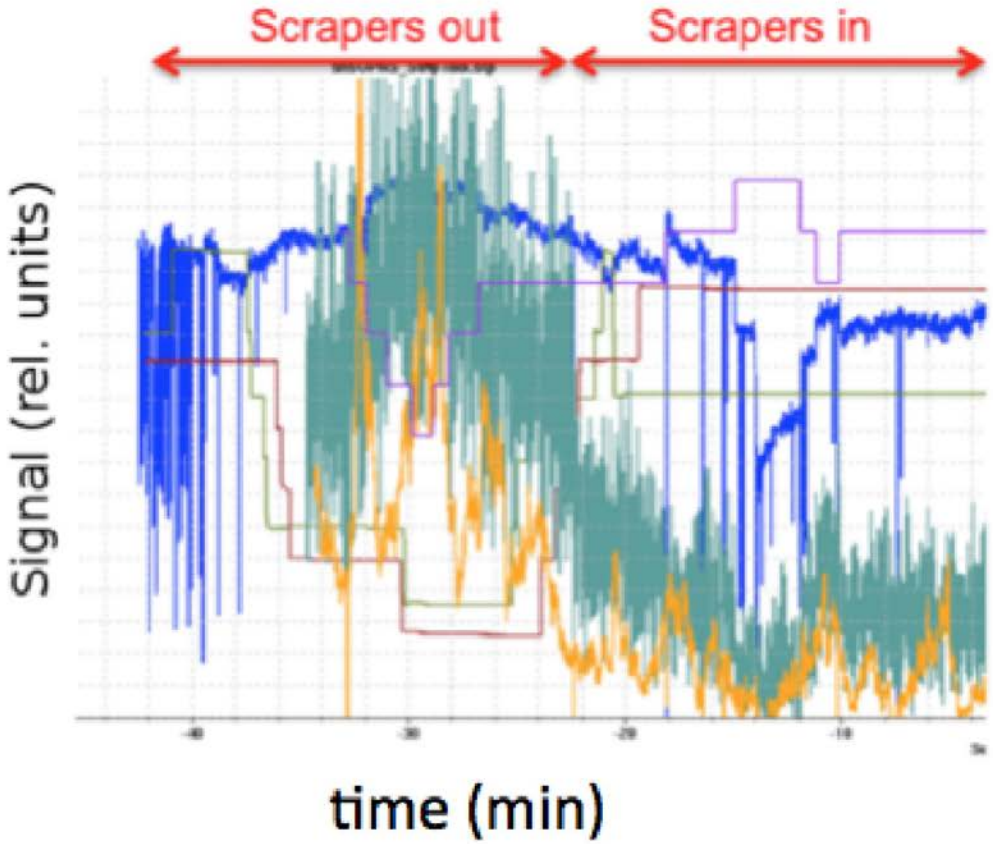

Fig. 19: Beam loss reduction due to low-energy scraping. Magenta, light green and violet show the scraper positions. Blue shows the beam charge, and orange and dark green show BLM signals. The beam loss is reduced by up to 50–60% at certain locations by scraping about 3% of the beam, primarily in the CCL, the beginning of the SCL and the ring injection dump beam line. Figure reproduced from Ref. [24].

(J. Galambos, Ramp up progress, SNS Accelerator Advisory Committee Meeting, 3 February 2010).

Beam Halo (cont.)

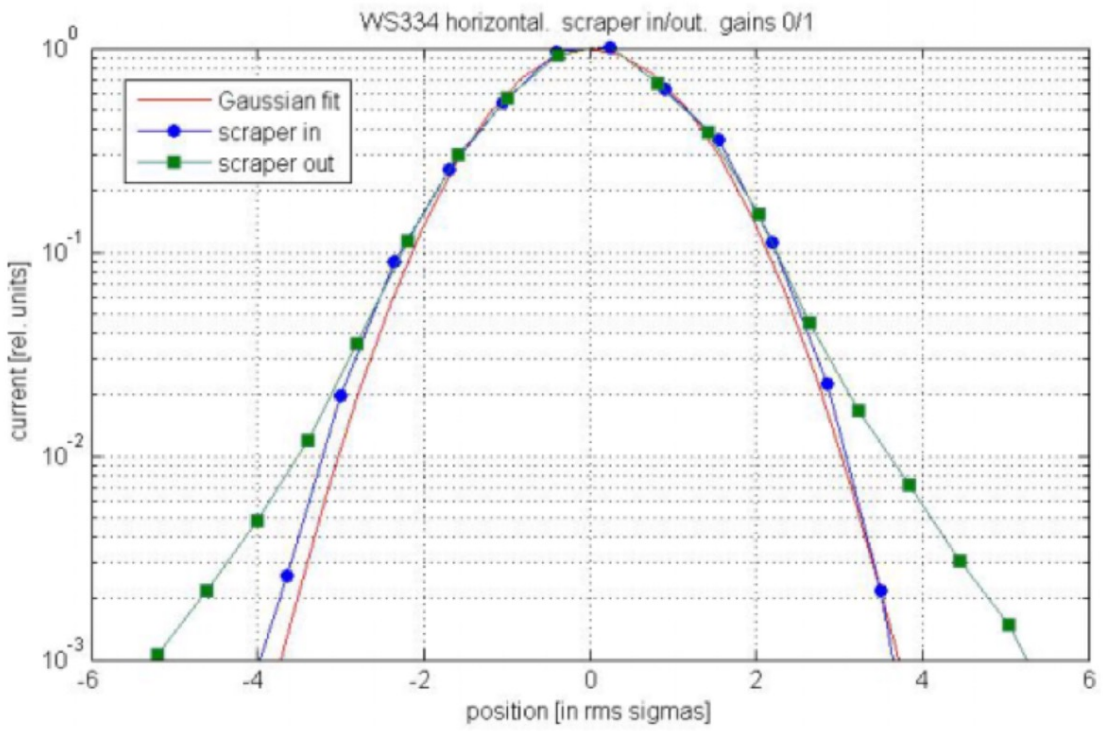

Fig. 21: A wire-scanner beam profile measurement in the DTL, before and after inserting the MEBT scrapers. The beam energy is 39.7 MeV. Blue circles—scraper is in; green squares—scraper is out; solid red line—Gaussian fit. Figure reproduced from Ref. [26].

(A. Aleksandrov et al. 2005 Particle Accelerator Conf.)

Beam Halo (cont.)

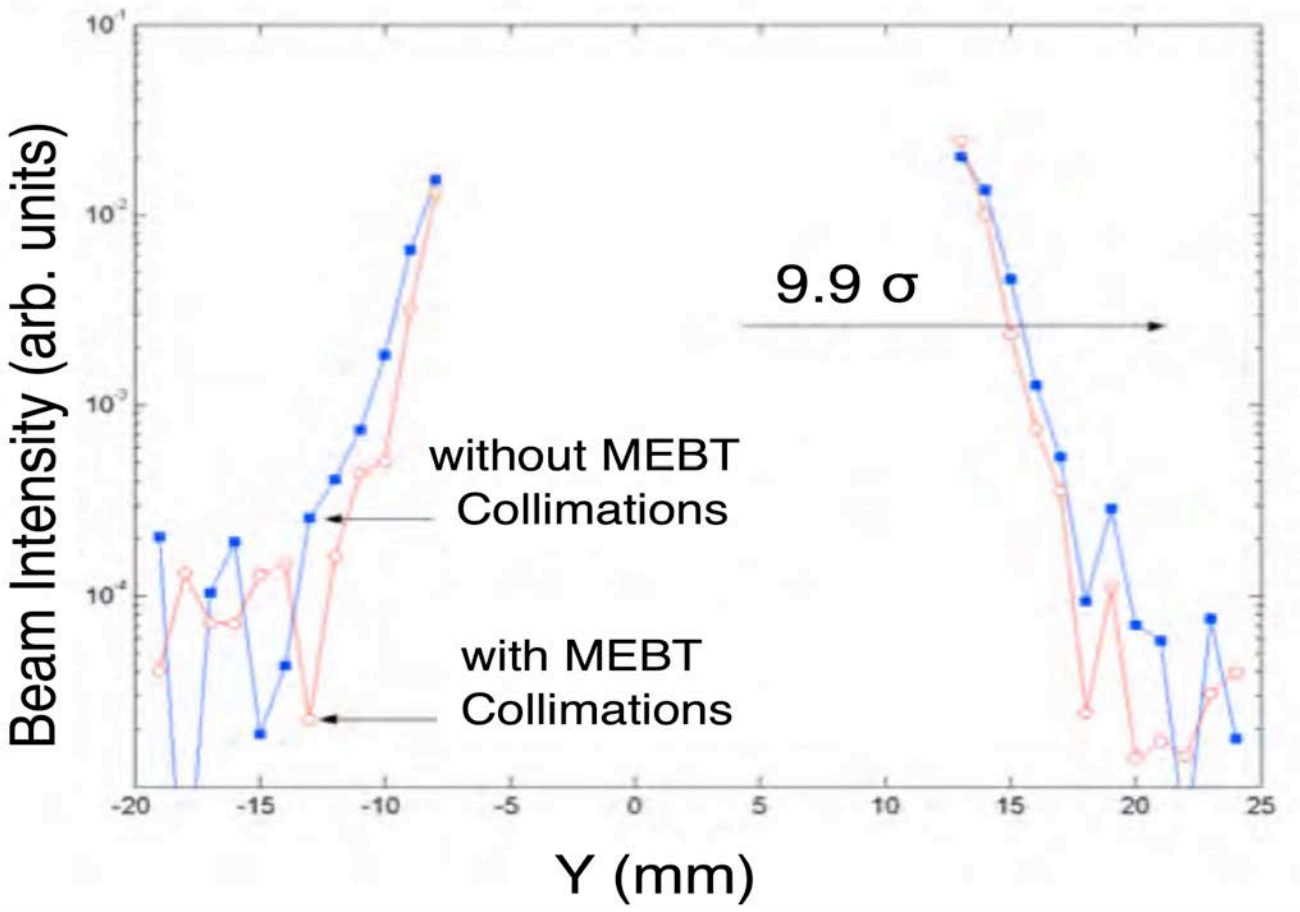

A wire scanner beam profile measurement in 1 GeV High Energy Beam Transport of SNS accelerator with and without MEBT scrappers (D. Jeon et al, SNS, 2010).

Beam Emittance Growth in Low Energy Beam Transport

RF Bunching

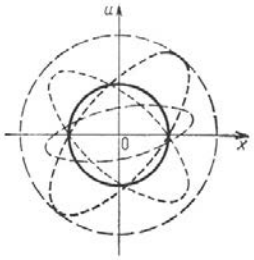

Beam	Emittance Growth $\varepsilon_{RF}/\varepsilon$
H^-	1.1 – 1.2
H^+	1.9 – 2.2

H^- Beam Chopping

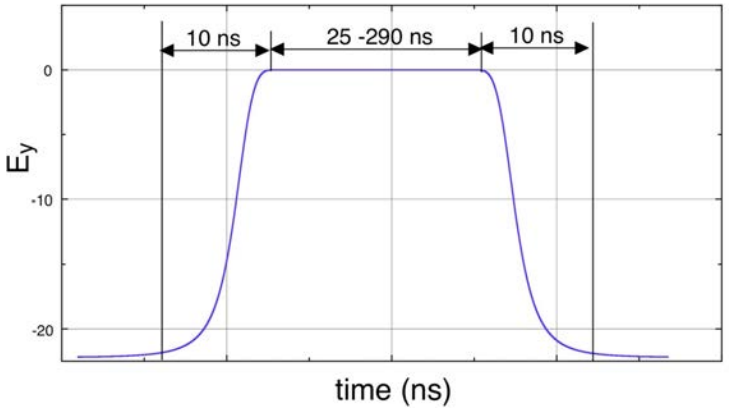

H^- Chopper Pulse	Emittance Growth $\varepsilon_{ch}/\varepsilon$
290 ns	1.1
36 ns	1.3

Bunchers Off

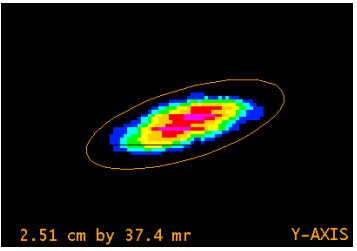

Bunchers On

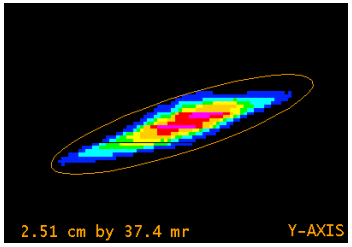

Chopper Off

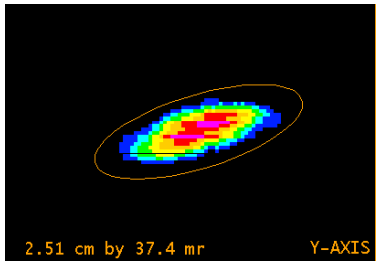

Chopper pulse 290 ns

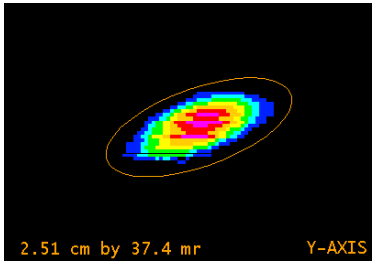

Chopper pulse 36 ns

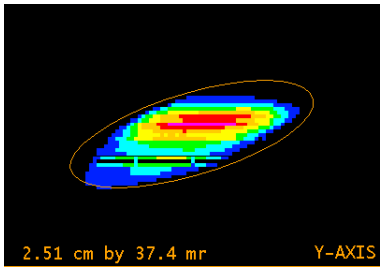

Emittance Growth due to Transverse-Longitudinal Coupling

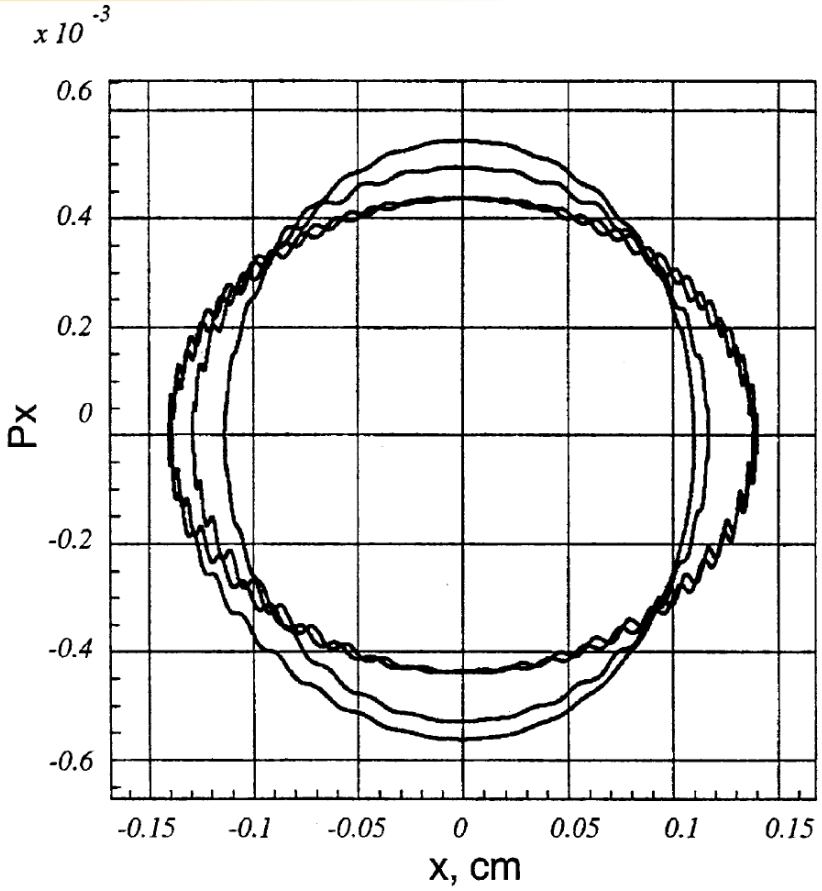

Phase space trajectory of particle in a standing wave RF accelerator.

Emittance Growth due to Transverse-Longitudinal Coupling (cont.)

Transverse oscillations in presence of RF field:

$$\frac{d^2X}{dt^2} + X[\Omega_{rs}^2 - \frac{\Omega^2}{2} h \sin(\Omega t + \psi_o)] = 0$$

Parameter h is proportional to amplitude of longitudinal oscillations Φ.

$$h = \Phi / \left| \mathrm{tg}\varphi_s \right|$$

Transverse oscillation equation for synchronous particle

$$\frac{d^2X}{dt^2} + \Omega_{rs}^2 X = 0$$

$$X = A\cos(\Omega_{rs} t + \psi_o)$$

Solution of equation for synchronous particle:

$$\dot{X} = -A\Omega_{rs} \sin(\Omega_{rs} t + \psi_o)$$

Synchronous particle performs oscillations along elliptical phase trajectory in phase space

$$\frac{X^2}{A^2} + \frac{\dot{X}^2}{\Omega_{rs}^2 A^2} = 1$$

Beam emittance

$$э = \frac{A^2 \Omega_{rs}}{\nu_s}$$

Emittance Growth due to Transverse-Longitudinal Coupling (cont.)

Maximum deviation from axis, A_{max}, is achieved by particles with minimal transverse oscillation frequency, while maximum spread in transverse momentum (and minimal amplitude A_{min}) is achieved by particles with maximal oscillation frequency

$$\Omega_{r\_\min} = \sqrt{\Omega_{rs}^2 - \frac{\Omega^2}{2}h}$$

$$\Omega_{r\_\max} = \sqrt{\Omega_{rs}^2 + \frac{\Omega^2}{2}h}$$

Non-synchronous particle performs transverse oscillations with variable transverse frequency while phase space area comprised by this motion is constant according to adiabatic theorem

$$э = \frac{A_{\max}^2 \Omega_{r\_\min}}{\nu_s} \qquad э = \frac{A_{\min}^2 \Omega_{r\_\max}}{\nu_s}$$

Effective emittance is limited by ellipse with semi-axes

$$э_{eff} = \frac{A_{\max} A_{\min} \Omega_{r\_\max}}{\nu_s}$$

$$X = A_{\max} \qquad \dot{X} = A_{\min}\Omega_{r\_\max}$$

$$\boxed{\frac{э_{eff}}{э} = \sqrt{\frac{\Omega_{r\_\max}}{\Omega_{r\_\min}}} \approx 1 + h\frac{\Omega^2}{4\Omega_{rs}^2}}$$

$$h = \Phi / \left|\mathrm{tg}\varphi_s\right|$$

With approaching parametric resonance condition $2\Omega_{rs} \sim \Omega$, emittance growth becomes more significant (R. Gluckstern, 1964):

$$\boxed{\frac{э_{eff}}{э} = 1 + h\left(\frac{\Omega^2}{4\Omega_{rs}^2 - \Omega^2}\right)}$$

Emittance Growth in Drift Tube Linac (0.75 MeV – 100 MeV)

Beam Capture in DTL 75% - 80%
Additional losses 0.1% -1%

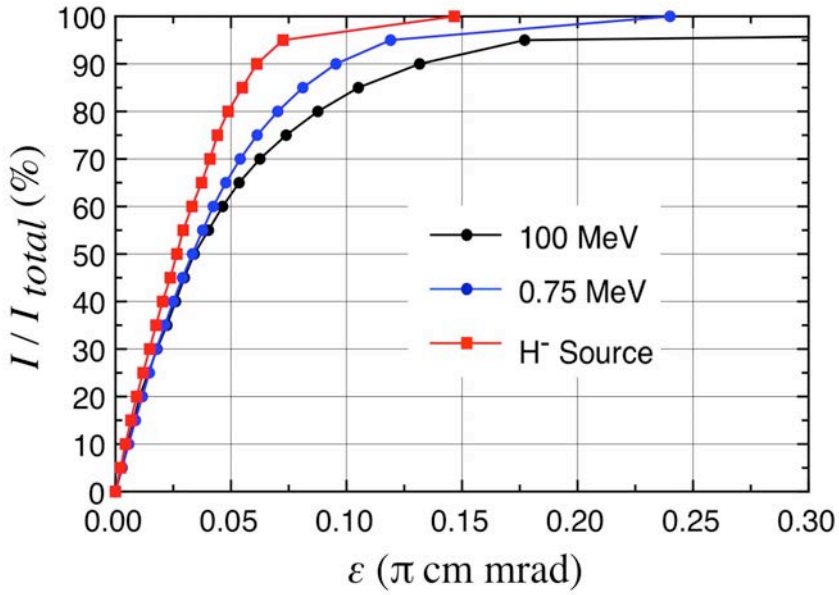

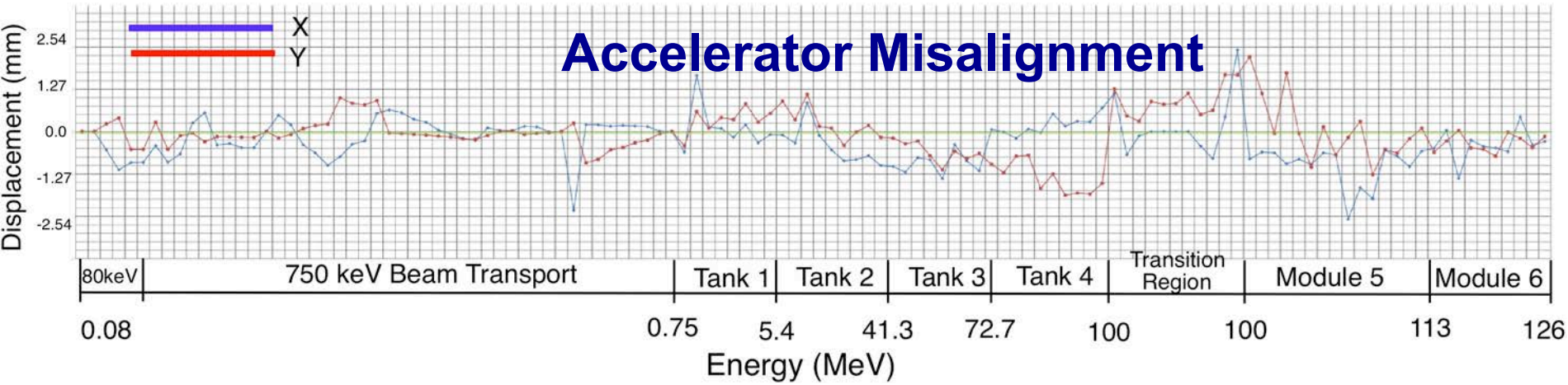

Dynamics of Uncaptured Particles in Drift Tube Linac

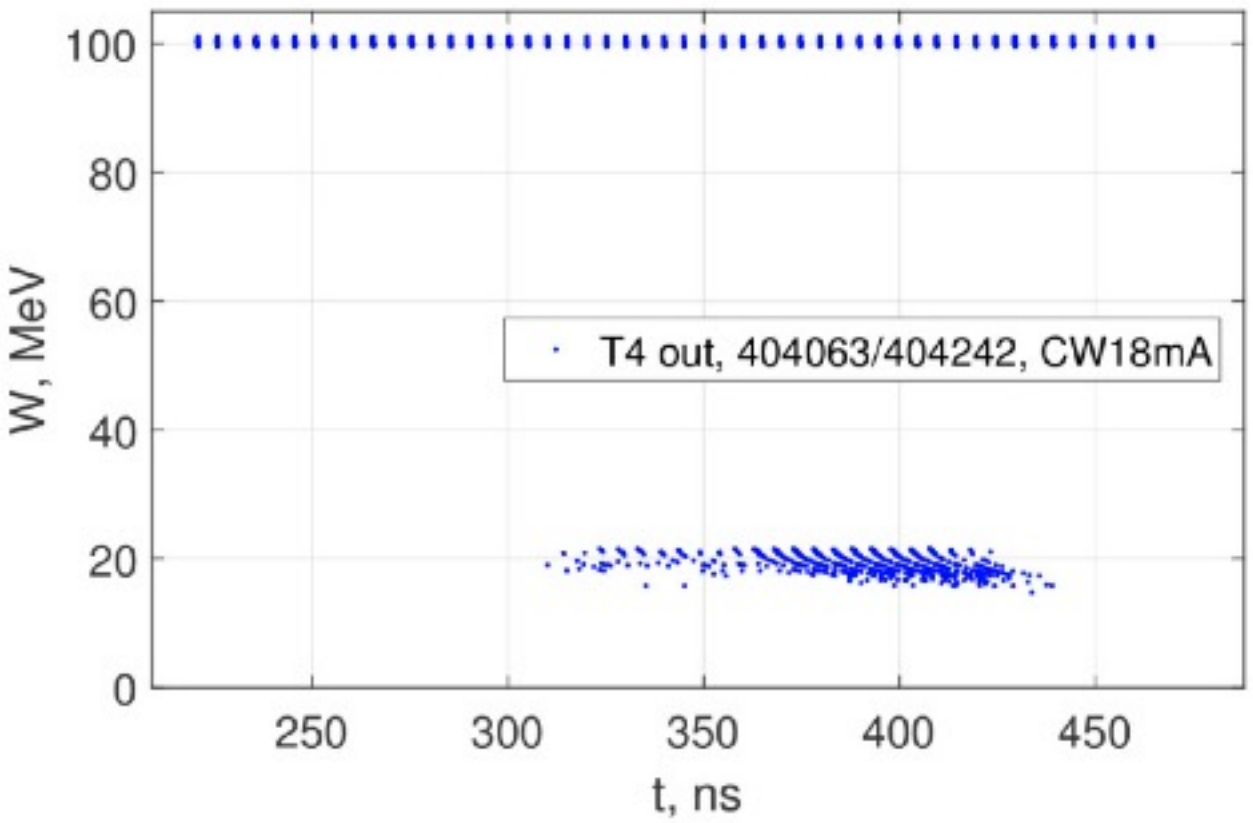

Distance between RF gaps: $L = n\beta\lambda$

***n=1* accelerated particles**

***n=2* non-accelerated particles**

Accelerated and non-accelerated particles after Tank 4 (S.Kurennoy, IPAC16)

Beam Capture in Tank 1 of LANSCE Drift Tube Linac

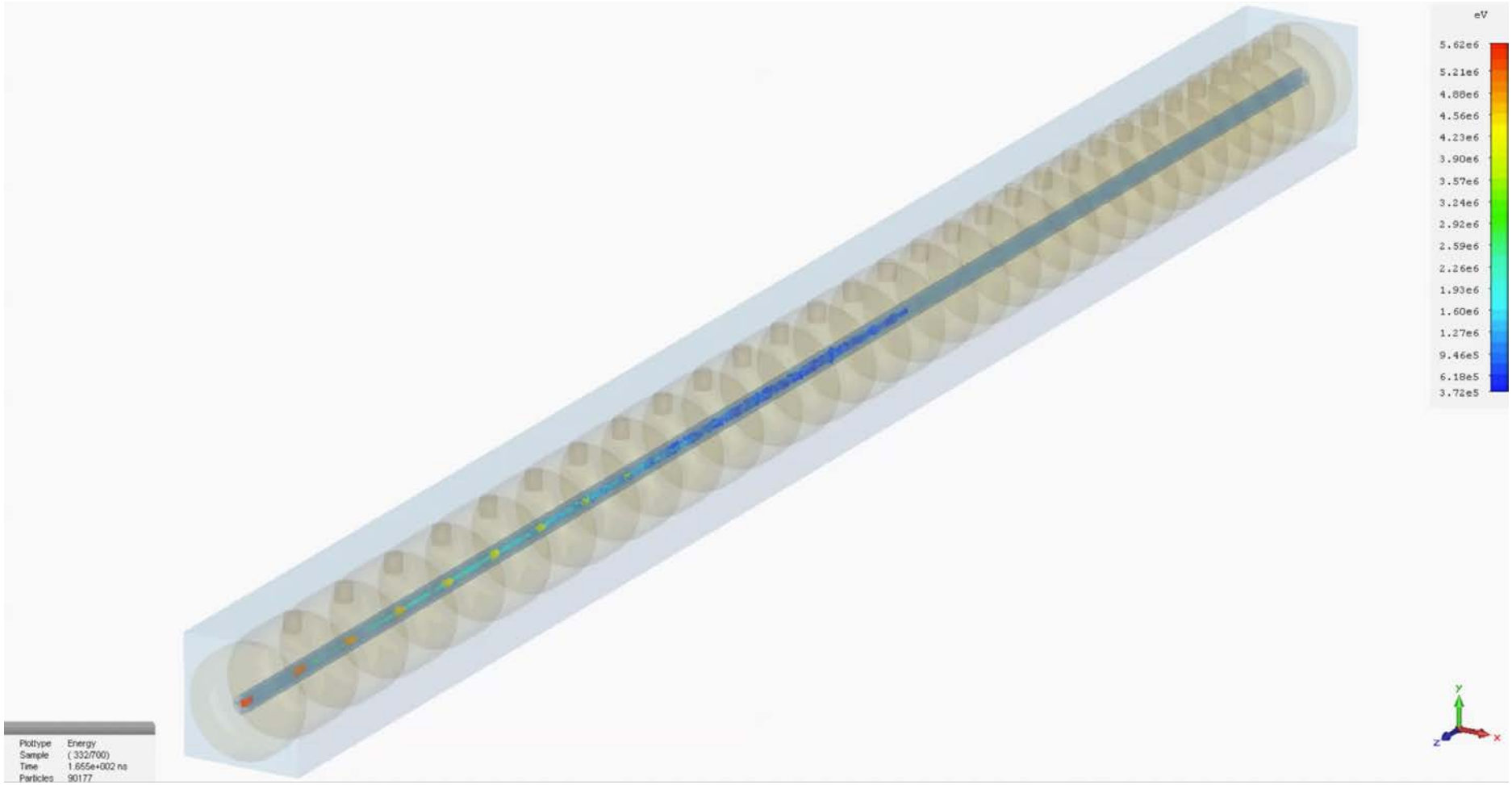

(Courtesy of Sergey Kurennoy)

Acceleration in Non-Ideal Accelerating Structure

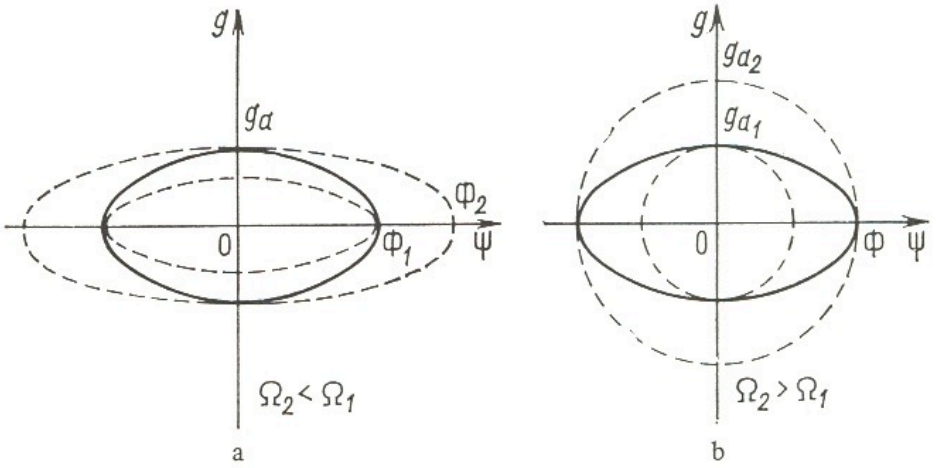

Fig. 1.12 Effect of an abrupt change in frequency on longitudinal oscillations of particles.

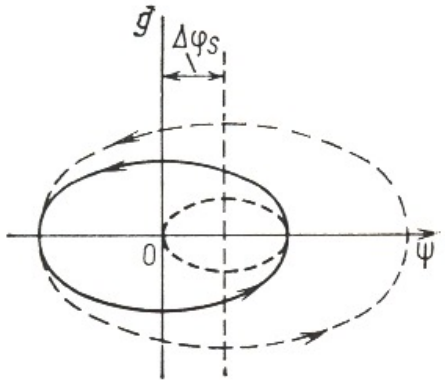

Fig. 1.10 Effect of an abrupt change of the equilibrium phase on the longitudinal oscillations of particles.

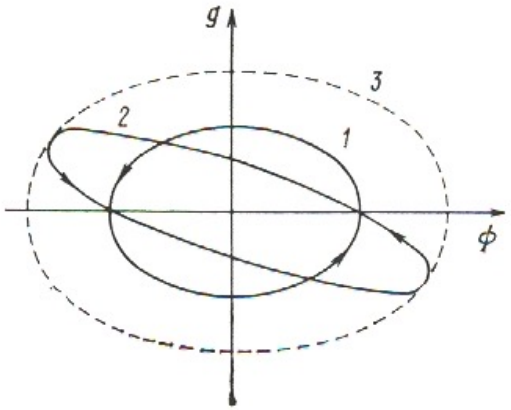

Fig. 1.11 Effect of an empty space on longitudinal oscillations of particles.

Acceleration in Non-Ideal Accelerating Structure (cont.)

Relative momentum deviation from synchronous particle

$$g = \frac{p - p_s}{p_s}$$

Dimensionless longitudinal oscillation frequency

$$\frac{\Omega}{\omega} = \sqrt{\left(\frac{qE\lambda}{mc^2}\right)\frac{|\sin\varphi_s|}{2\pi\beta\gamma^3}}$$

Dimensionless acceleration rate

$$W_\lambda = \frac{eE_oT\lambda\cos\varphi_s}{mc^2}$$

Increase in relative momentum spread

$$\langle \Delta g_a \rangle = \sqrt{\frac{N}{2}\left[\langle \delta g \rangle^2 + \left(\frac{\Omega}{\omega}\right)_N^2 \langle \delta\psi \rangle^2\right]},$$

$$\langle \delta\psi \rangle = 2\pi \left\langle \frac{\delta z}{\beta\lambda} \right\rangle;$$

$$\langle \delta g \rangle = \frac{kW_\lambda}{\beta_N} \sqrt{\left\langle \frac{\delta E_0}{E_0} \right\rangle^2 + 4\pi^2 \operatorname{tg}^2\varphi_s \left\langle \frac{\delta z}{\beta\lambda} \right\rangle^2}.$$

Acceleration in Non-Ideal Accelerating Structure (cont.)

For LANL 805-MHz linac

$$<\delta(\frac{\Delta p}{p})>=\sqrt{\frac{N_a}{2}(1.5\cdot 10^{-7}<\frac{\delta E_o}{E_o}>^2+4.6\cdot 10^{-6}<\delta\psi>^2)}$$

Typical momentum spread: $\Delta p/p = 8\text{x}10^{-4}$.

For instability of the RF field amplitude and phase

$$<\delta E_o / E_o>\approx 1\% \qquad <\delta\psi>\approx 1^o$$

estimated increase of momentum spread of the beam

$$<\delta(\Delta p / p)>\approx 1.7\cdot 10^{-4}$$

Beam Energy Spread Measurements

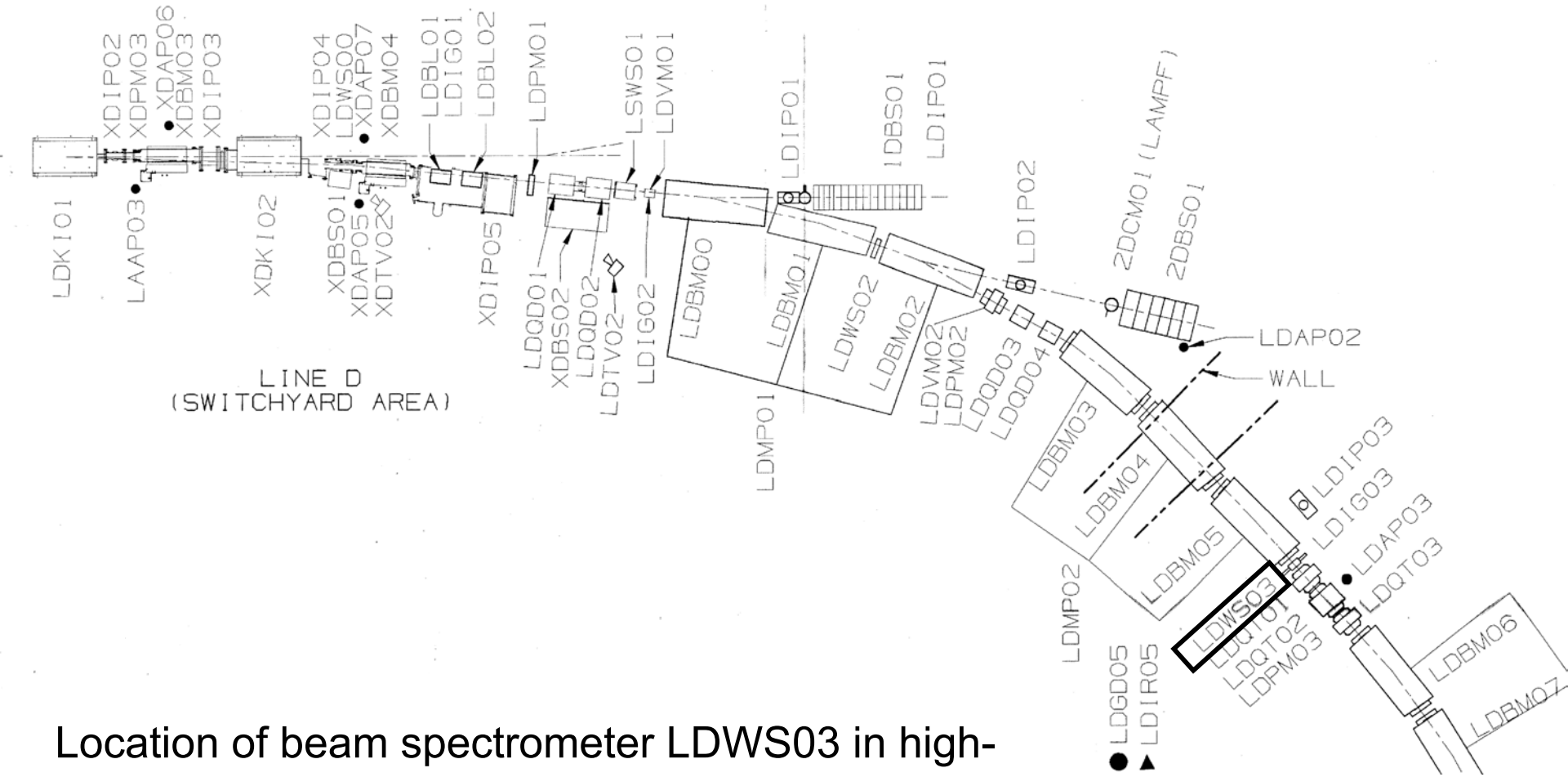

Location of beam spectrometer LDWS03 in high-energy part of accelerator facility

Beam Energy Spread Measurements (cont.)

Beam Momentum Spread

$$\frac{\Delta p}{p} = \frac{\sqrt{R_x^2 - \beta_x(4\,э_{x\_rms})}}{\eta}$$

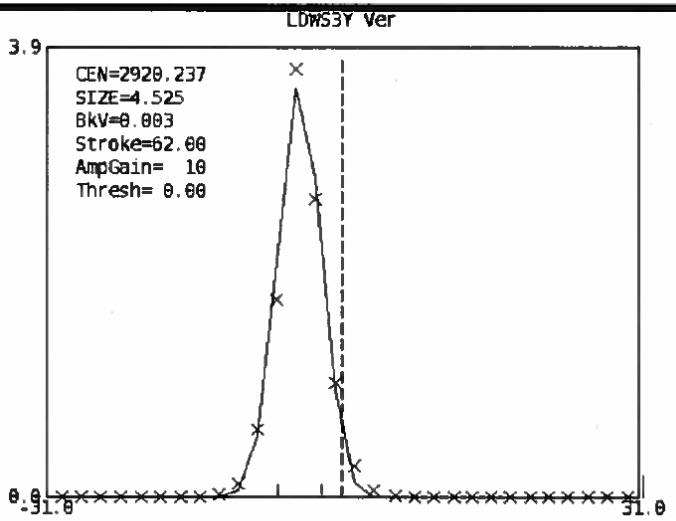

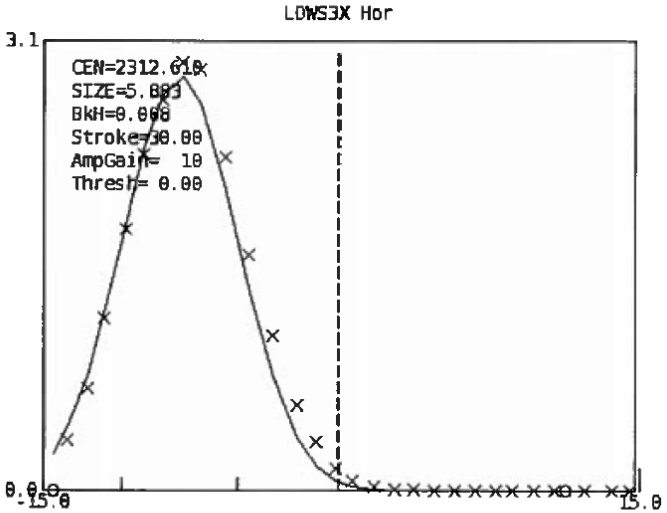

$R_x = 0.5793$ cm

$\beta_x = 1.11236$ cm /mrad

$э_{x\_rms} = 0.04\ \pi$ cm mrad

$\eta = 4.8798$ m

$$\frac{\Delta p}{p} = 8.13 \cdot 10^{-4}$$

Background Avg = 4, Data Avg = 10, NBins = 30, Mode = STEP, Algorithm = Gauss 0.0, Sequential Scan
WSPSR Wire Scanners -- 2017.01.30-13:02:23.023, Beam Gate = SRT0, Rep Rate = 4, DWSS = 1174, SWSS = 1174, WSDT = 1618

Beam Energy Spread Measurements (cont.)

(a)

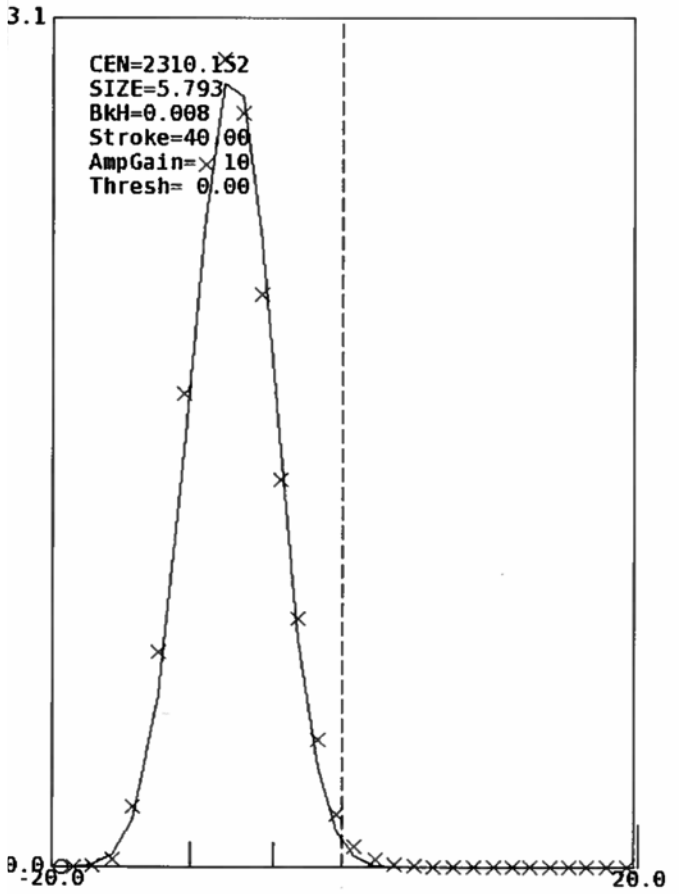

(b)

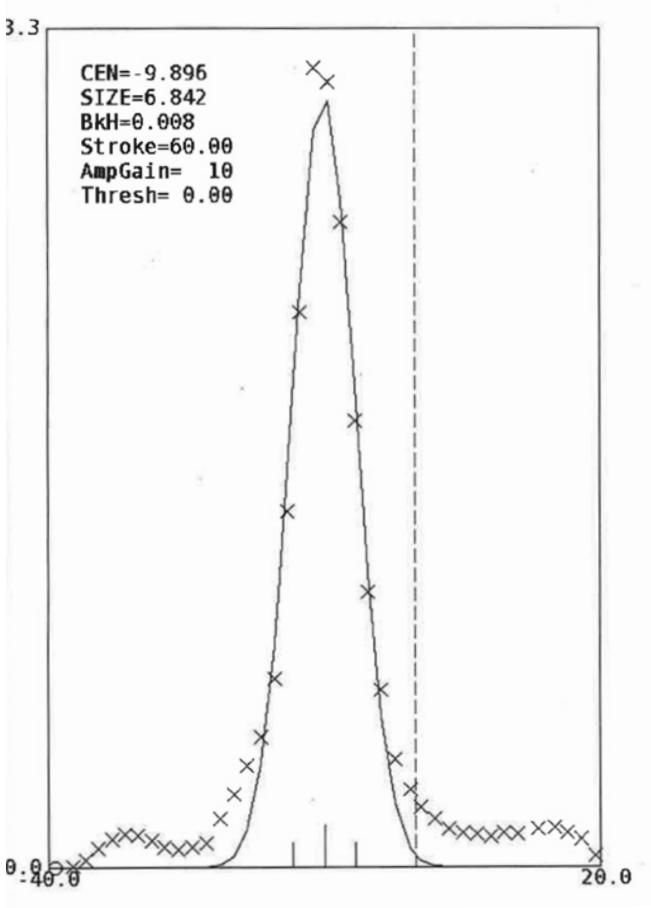

Momentum spread of the beam measured by LDWS03 wire scanner: (a) properly tuned beam, (b) beam with momentum tails due to improper tune.

Effect of DTL Cavity Field Error on Beam Losses

Maximum Spill ≈ $10^{n*Error}$ where n = 3 - 4

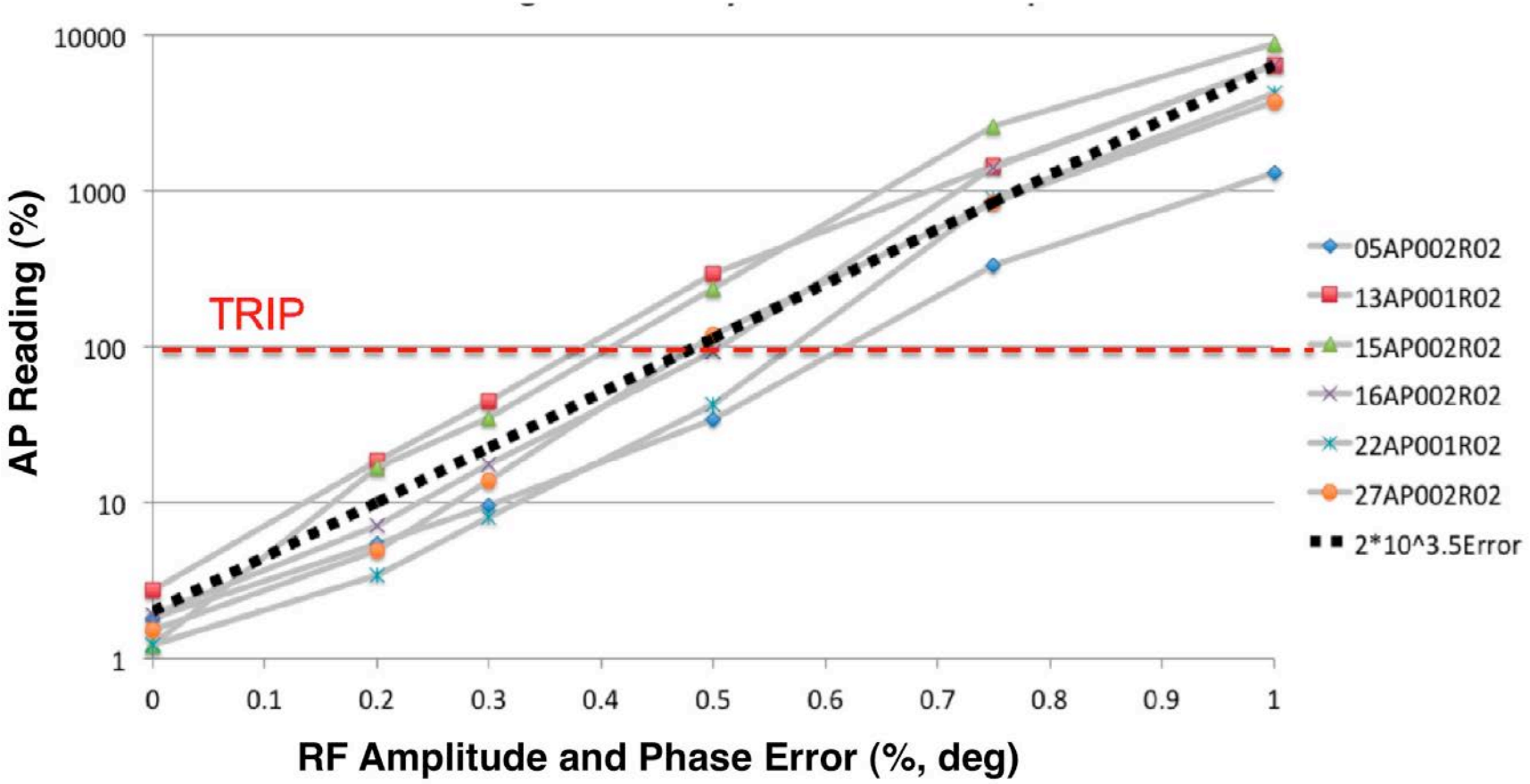

(L.Rybarcyk et al, LINAC 2016)

Observation of Low-Momentum Beam Spill

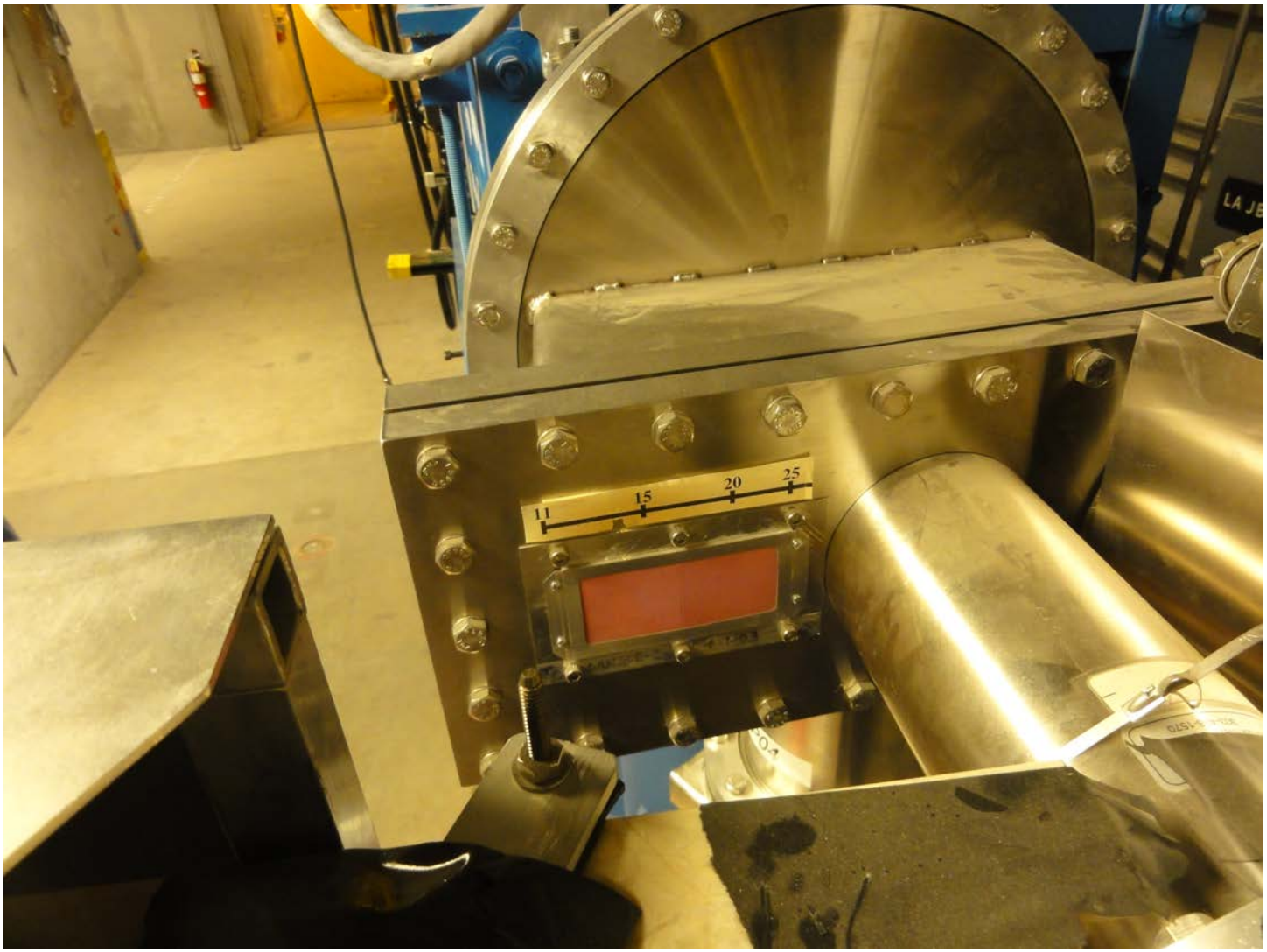

Observation of Low-Momentum Beam Spill

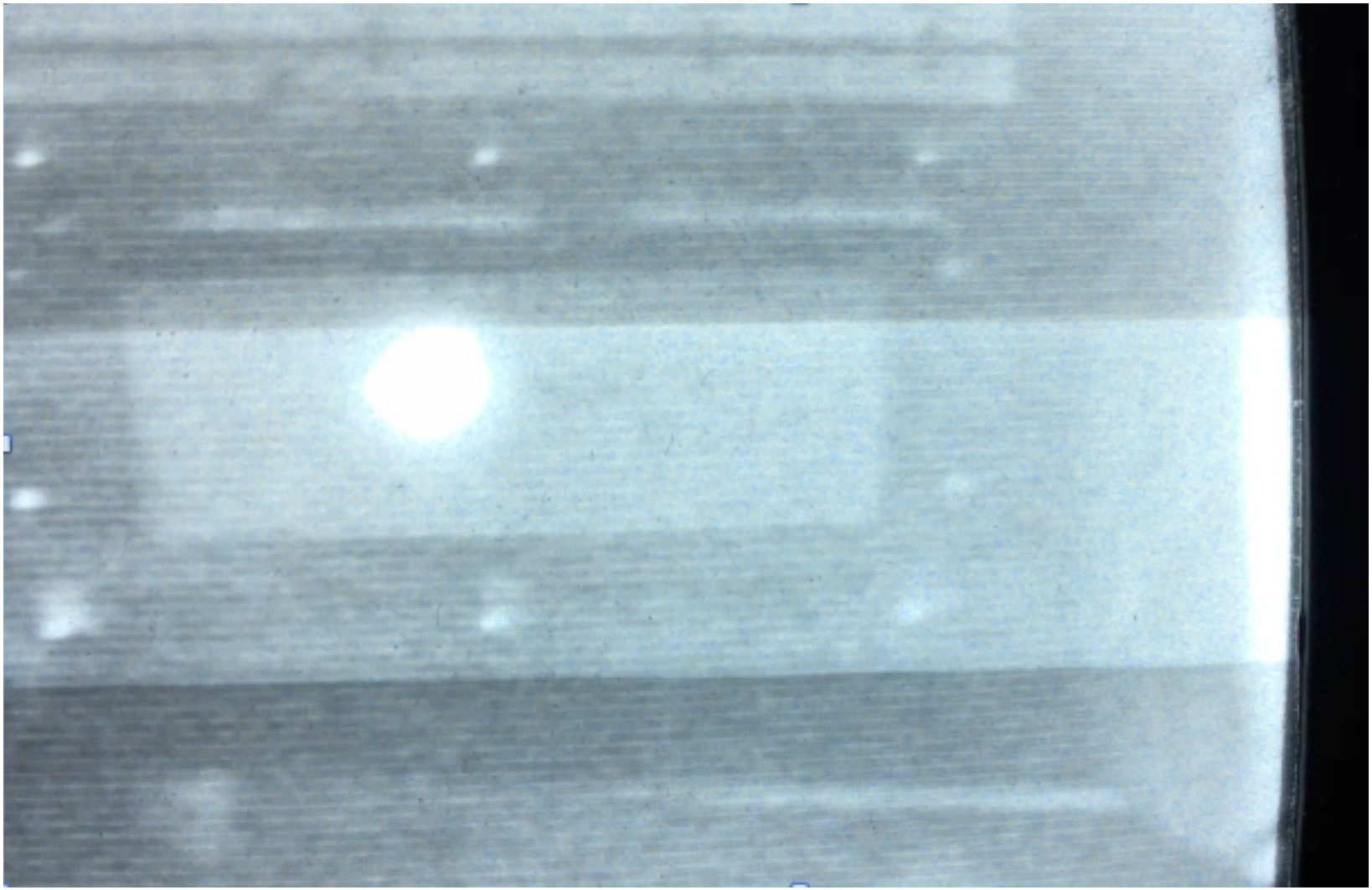

Transverse Oscillations in Non-Ideal Focusing Structure

Misalignments and lattice errors can significantly affect beam dynamics. Consider equation for beam ellipse

$$A^2 = x^2 + \beta_x^2 x'^2$$

where β_x is the value of beta-function in the middle of quadrupole. Suppose, particle trajectory experience random kick in phase space dx dx'. Increase of beam size is

$$d(A^2) = (dx)^2 + \beta_x^2 (dx'^2)$$

In smooth approximation, particle trajectory is $x \approx x_o \sin(\Omega_r t + \Phi_{ox})$, $x' \approx x_o \Omega_r \cos(\Omega_r t + \Phi_{ox})$. After averaging over all phases Φ_{ox}, increase of particle oscillation amplitude is determined by

$$< dA >^2 = \frac{1}{2}[< dx >^2 + \beta_x^2 < dx' >^2]$$

The distortion of beam amplitude of oscillations after N_Q quadrupoles can be written as

$$< \Delta A > = \sqrt{\frac{N_Q}{2}[\Sigma < \Delta x >^2 + \Sigma < \Delta x' >^2 \beta_x^2]}$$

where summation is taken over all sources of distortion at each focusing period.

Transverse Oscillations in Non-Ideal Focusing Structure

Rms increase of amplitude of transverse oscillations

$$\langle \Delta A \rangle = \sqrt{\frac{N_\Phi}{2}\left[\Sigma \langle \Delta x^* \rangle^2 + \frac{1}{\nu_\Phi^2}\Sigma \langle \Delta \dot{x}^* \rangle^2\right]}.$$

1) slope of longitudinal axis of the lens

$$\langle \Delta x^* \rangle = a_1 K^2 \langle \Delta r_K \rangle; \quad \langle \Delta \dot{x}^* \rangle = b_1 K^2 \langle \Delta r_K \rangle;$$

2) parallel shift of axis of the lens

$$\langle \Delta x^* \rangle = a_2 K^2 \langle \Delta r_0 \rangle; \quad \langle \Delta \dot{x}^* \rangle = b_2 K^2 \langle \Delta r_0 \rangle;$$

3) rotation of transverse axes of the lens

$$\langle \Delta x \rangle^* = 4 a_2 K^2 A \sqrt{\overline{(\Delta\psi)^4}}; \quad \langle \Delta \dot{x}^* \rangle = 4 b_2 K^2 A \sqrt{\overline{(\Delta\psi)^4}};$$

For FODO Structure

$$a_1 = \frac{1}{3\sqrt{2}}\left[1 + \frac{K^2}{4}\left(1 + 2\frac{g}{D}\right)\right]^{1/2};$$

$$b_1 = \frac{K^4}{\sqrt{2}} 10^{-2}\left[1 + \left(1 + 6\frac{g}{D}\right)^2\right]^{1/2};$$

$$a_2 = \left[\left(1 + \frac{g}{D}\right)^2 - \frac{K^2}{6}\left(1 + \frac{5}{2}\frac{g}{D} + \frac{3}{2}\frac{g^2}{D^2}\right)\right]^{1/2};$$

$$b_2 = \sqrt{2}\left[1 - \frac{K^2}{4}\left(1 + 2\frac{g}{D}\right)\right]^{1/2}.$$

$K = D\sqrt{\frac{qG}{mc\beta\gamma}}$ Quadrupole strength

$\frac{g}{D}$ Ratio of drift space to lens length

$\upsilon_\phi \approx$ phase advanve

Δr_o shift of axis of the lens

Δr_k Shift of the end of magnetic axis

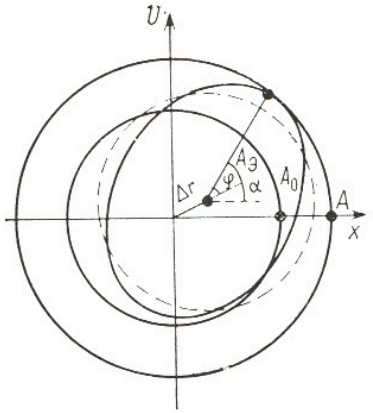

Fig. 2.15 Effective emittance caused by random beam perturbations.

Emittance Growth due to Nonlinearities

In a perfect linear focusing channel, random fluctuation do not result in emittance growth. However, in presence of lattice field nonlineraities, emittance growth is unavoidable due to filamentation in phase space.

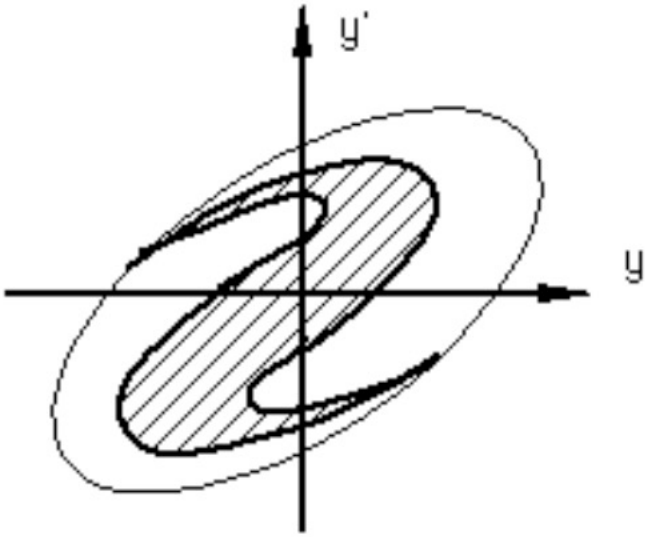

(c) Filamenting beam

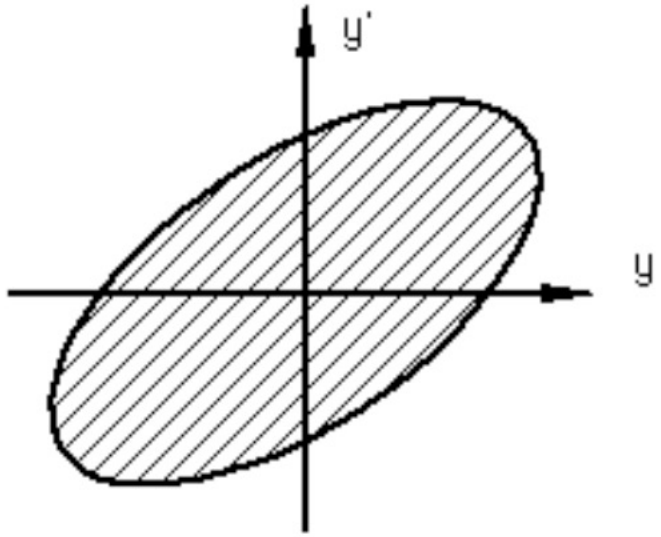

(d) Fully filamented beam

Effect of Random Errors on Emittance Growth in Presence of Nonlinearities

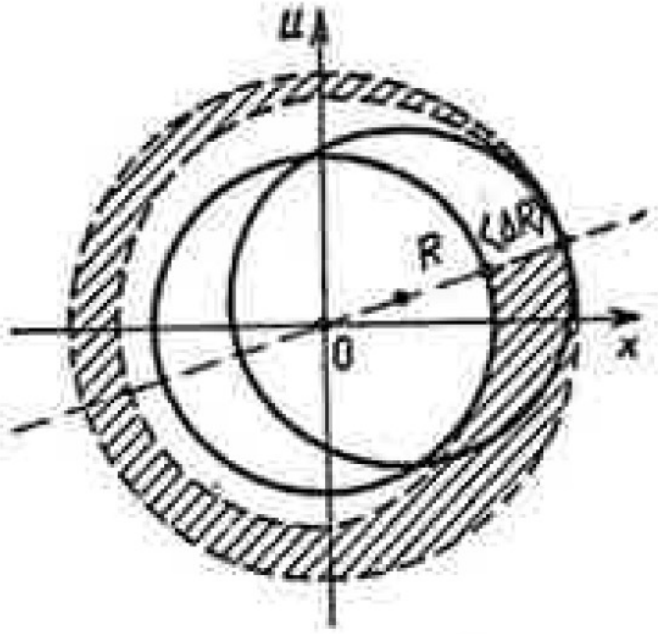

Spreading of effective emittance due to coherent perturbation of the beam in presence of frequency dispersion.

In ideal linear focusing field, beam emittance rotates collectively, and random errors do not result in beam emittance growth.
In presence of frequency dispersion, $d\mu / dR \neq 0$ effective emittance will increase.

If δA is an amplitude perturbation per period, then emittance growth per focusing period:

$$\frac{d\varepsilon}{dn} = 2\beta\gamma \frac{\mu_s R}{S} < \delta A >^{4/3} \sqrt[3]{\frac{1}{2\pi}\left(\frac{d\mu}{dR}\right)}$$

The peripheral part of the emittance increases significantly and the beam halo fill the entire acceptance of accelerator.

Beam Matching

Beam matching is determination of conditions for providing periodic beam envelopes in periodic accelerator structure.

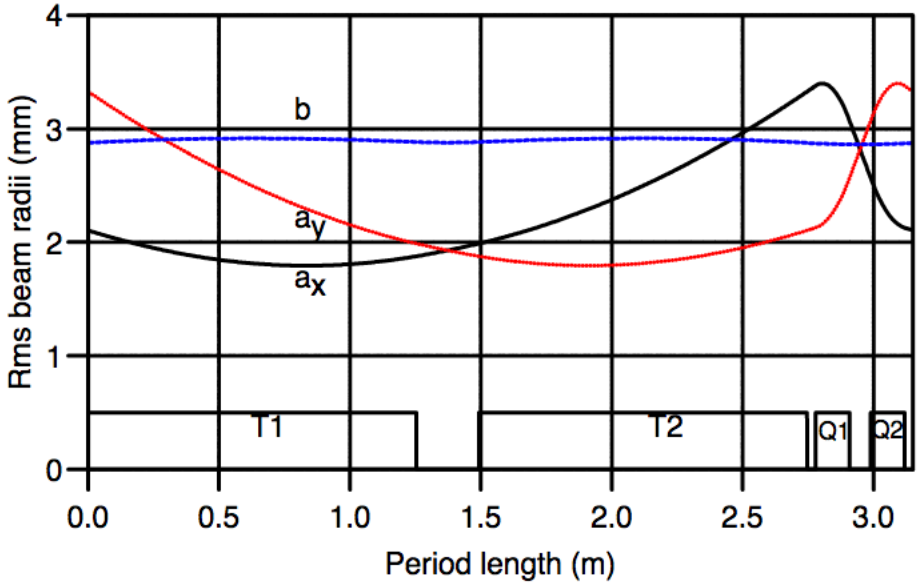

The matched beam radii along one period. T1,T2 bunching cavities, Q1, Q2 quadrupoles (Pabst, EPAC98).

Matched Beam Conditions

Matched beam conditions (see Section 6, slide 28)

$$R = \sqrt{\frac{\varepsilon S}{\beta\gamma\,\mu_t}}$$

$$R_x(z) = R[1 + \upsilon_{\max}\sin(2\pi\frac{z}{S})]$$

$$R_y(z) = R\,[1 - \upsilon_{\max}\sin(2\pi\frac{z}{S})]$$

$$R_z = \sqrt{\frac{\varepsilon_z S}{\beta\gamma^3\,\mu_z}}$$

Depressed transverse and longitudinal phase advances per unit length

$$(\frac{\mu_t}{S})^2 = (\frac{\mu_s}{S})^2 - \frac{3}{2}\frac{I}{I_c(\beta\gamma)^3}(\frac{\beta\lambda}{R_z R^2})(1 - M_z)$$

$$(\frac{\mu_z}{S})^2 = (\frac{\mu_{oz}}{S})^2 - 3\frac{I}{I_c(\beta\gamma)^3}(\frac{\beta\lambda}{R_z\,R^2})M_z$$

Keeping μ_s / S and μ_{oz} / S constant at transition from one accelerator section to another and making them changing adiabatically is the way to keep beam matched along machine.

Current - Independent Beam Matching

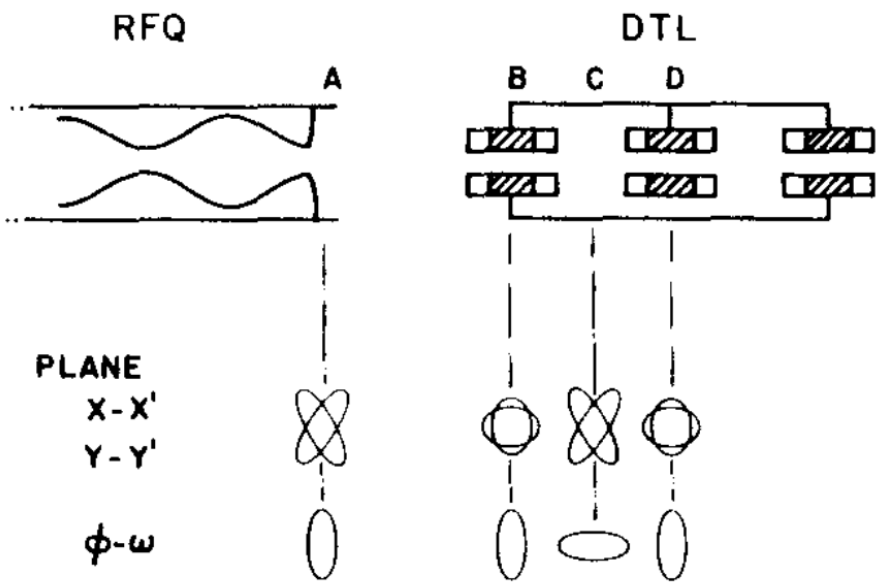

Schematic representation of matched phase spaces at end of RFQ (A), and at mid quad (B and D) and gap (C) in DTL.

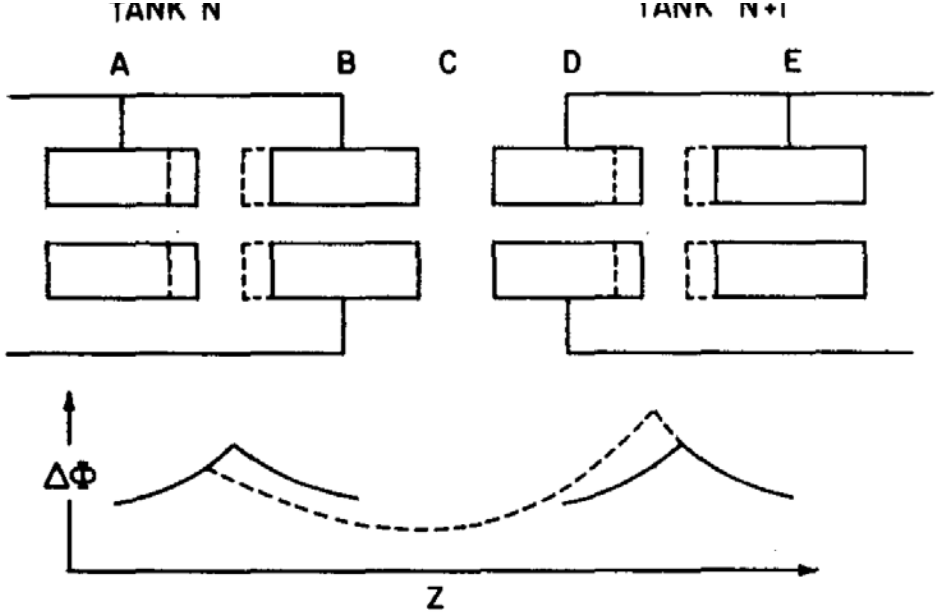

Longitudinal matching between DTL tanks. Solid lines show normal drift tubes and phase profiles. Dashed lines show modified drift tubes and resulting change in phase profile.

(R. S. Mills, K. R. Crandall, LINAC 84)

The accelerator lattice should be a continuous focusing structure that changes adiabatically along the machine. This allows the beam - originally matched within the RFQ - to continue to be approximately matched along the linac, and to remain nearly independent of the space charge and emittance of the beam.

Beam Matching

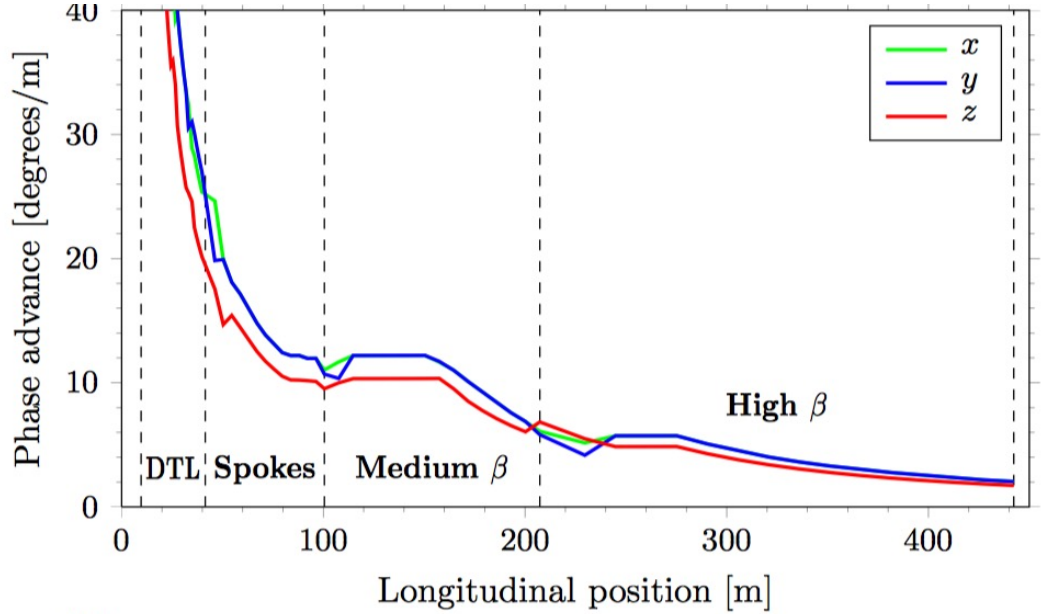

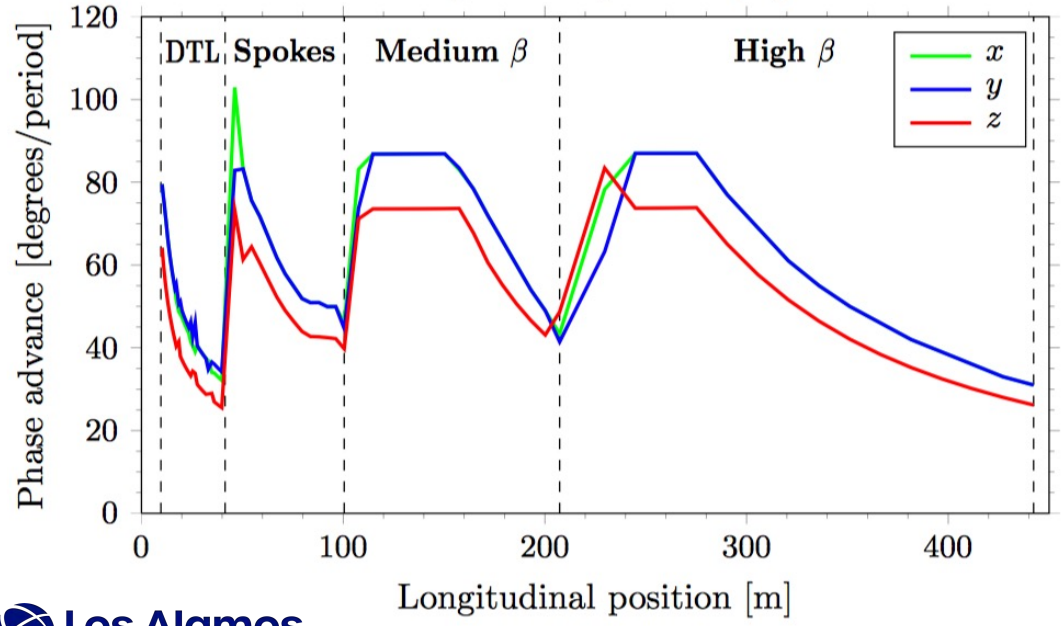

The ESS accelerator rate of phase advance in the three degrees of freedom, from the DTL to the end of the high-β section.

Phase advance per meter.

Phase advance per lattice cell.

Effect of Beam Mismatch

Matched Beam

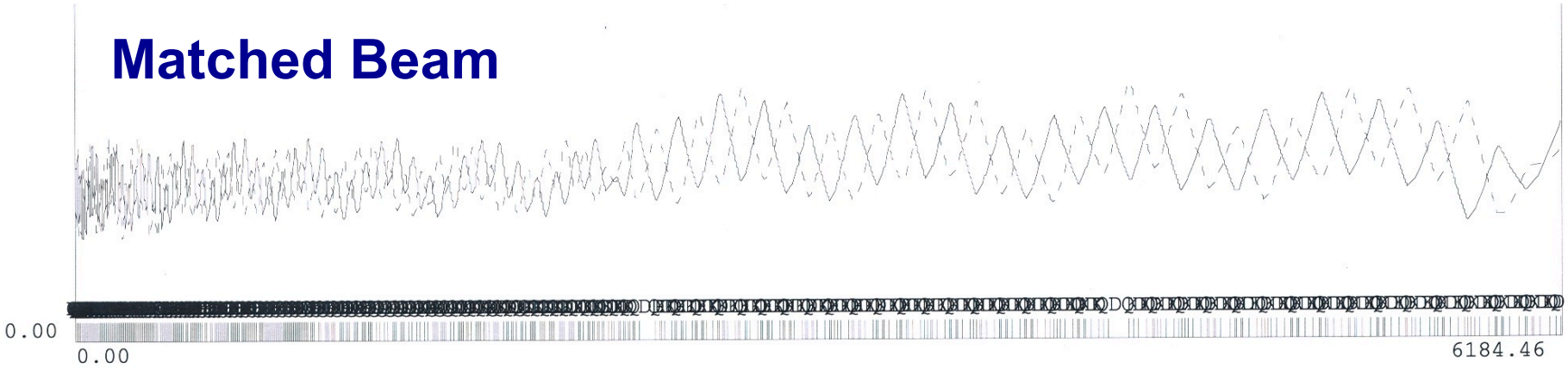

Mismatched Beam

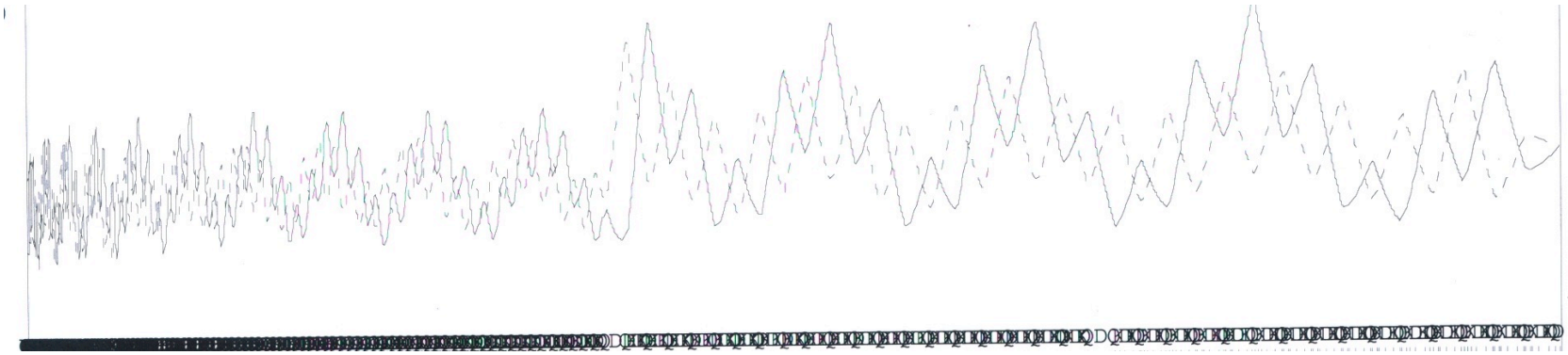

Effect of Beam Mismatch at the Entrance of DTL on Beam Loss in Transition Region (100 MeV)

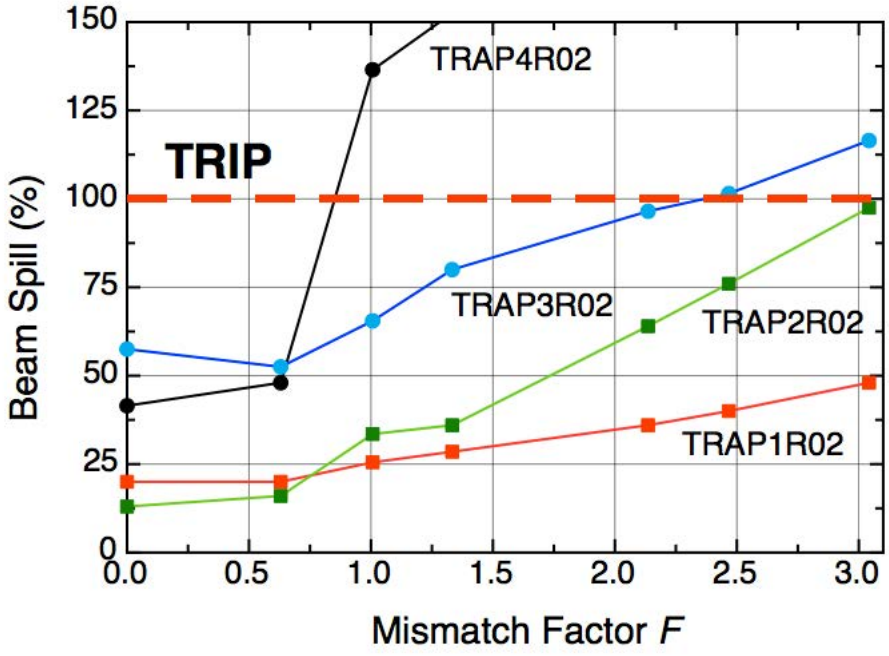

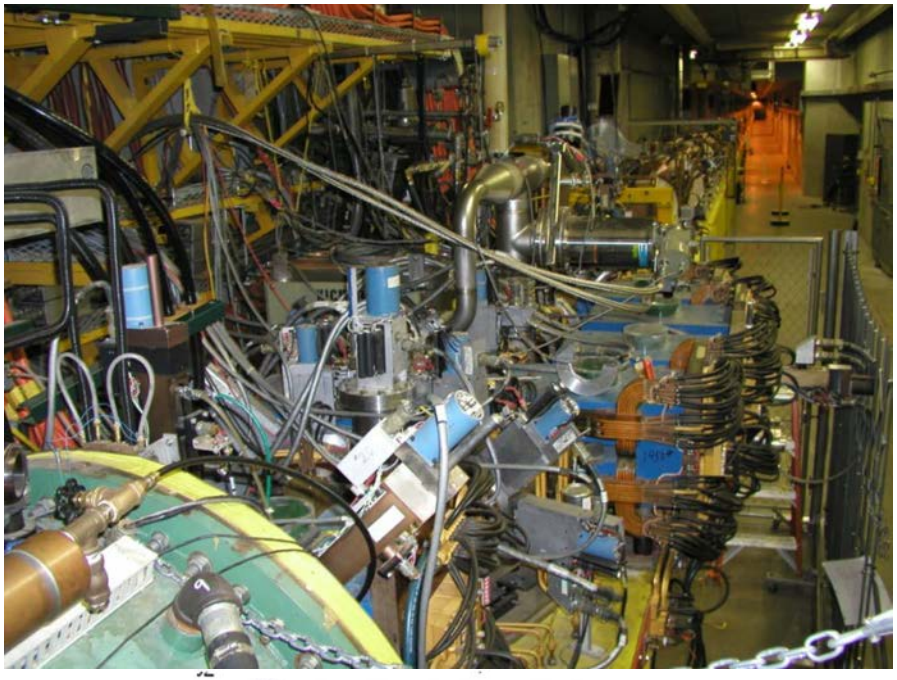

Mismatch Factor:

$$F = \sqrt{\frac{1}{2}(R + \sqrt{R^2 - 4})} - 1$$

Ellipse Overlapping Parameter:

$$R = \beta_1\gamma_2 + \beta_1\gamma_2 - 2\alpha_1\alpha_2$$

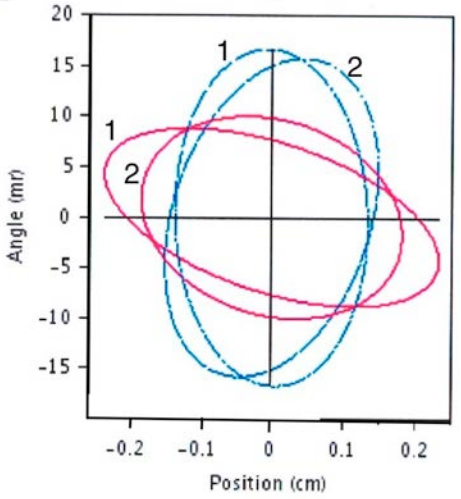

$F = 0.6$

Collimation of Beam Phase Space

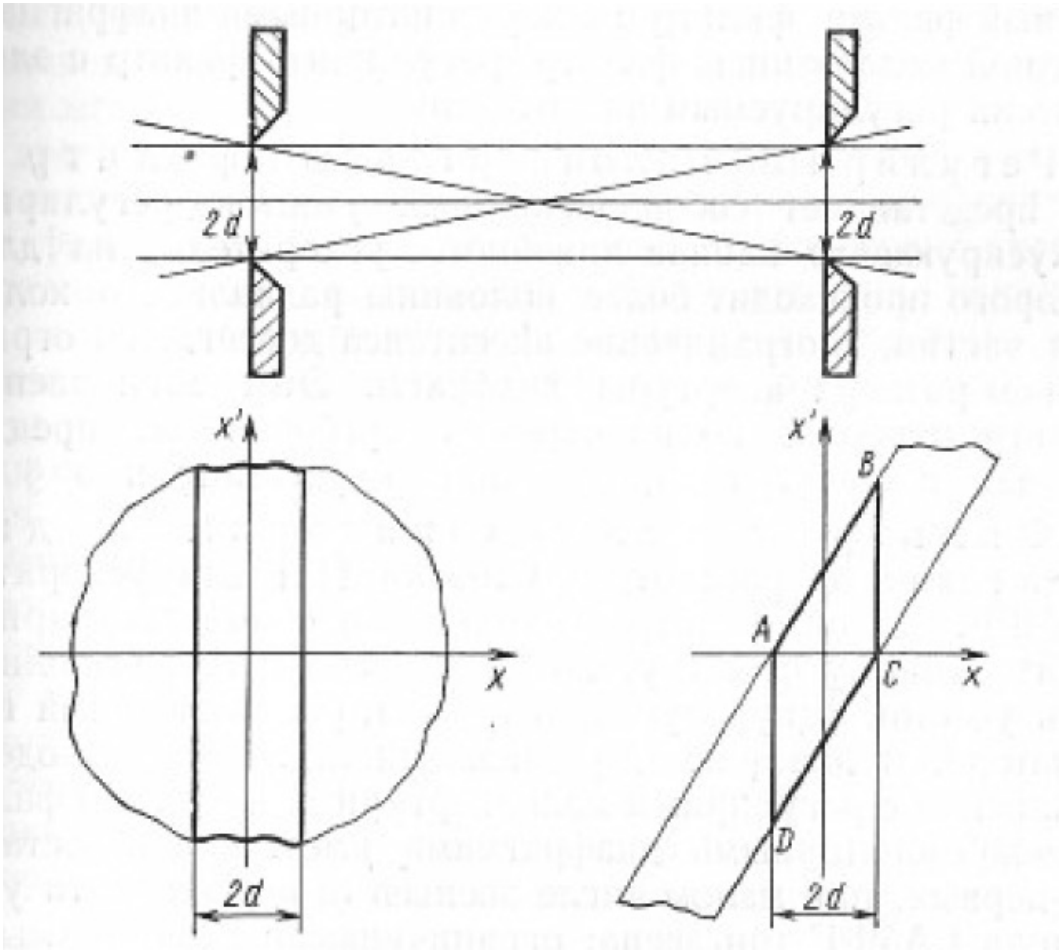

Transverse Beam Dynamics in Drift Tube Linac

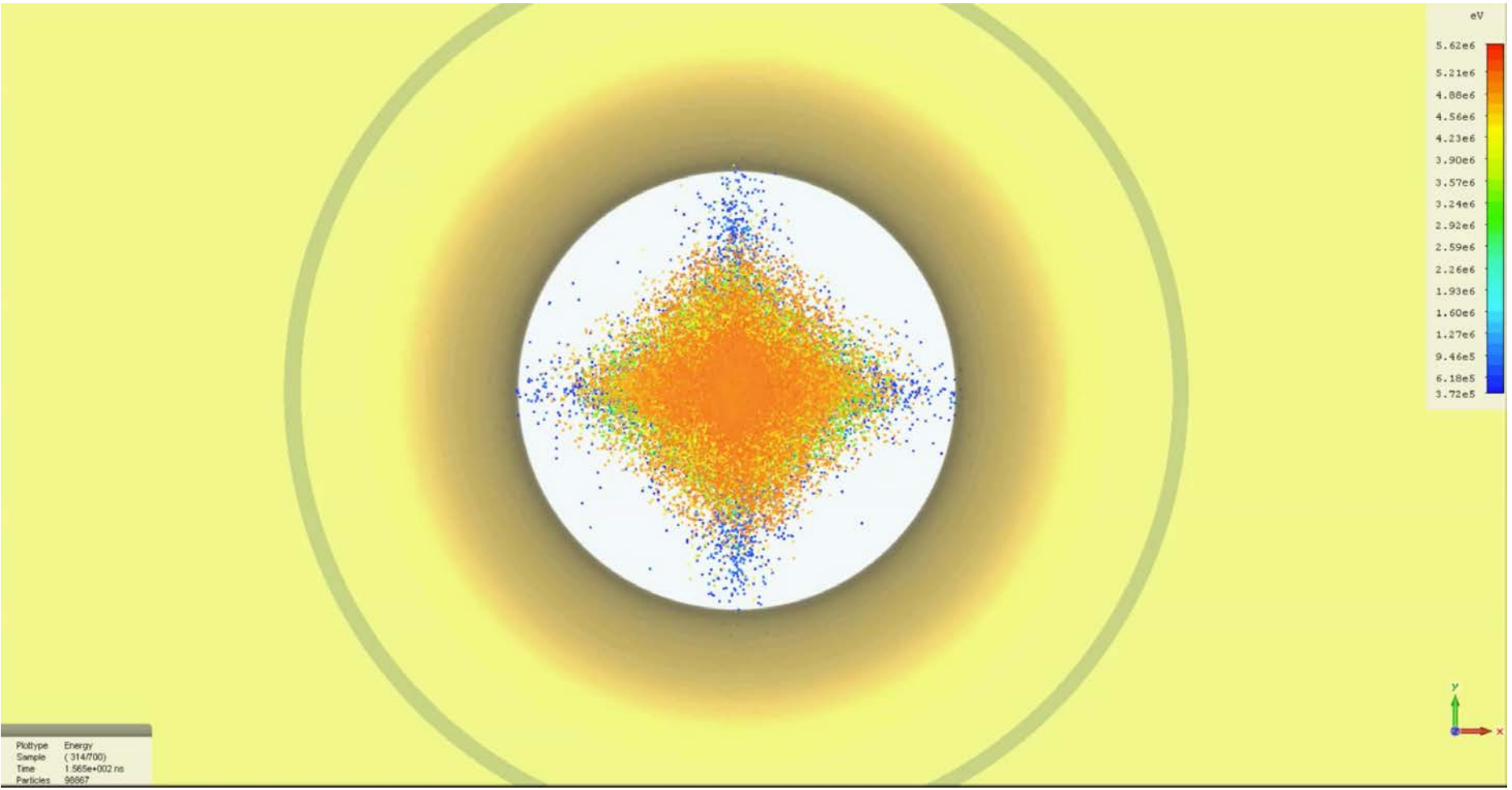

(Courtesy of Sergey Kurennoy)

Beam Losses versus Lattice Phase Advance

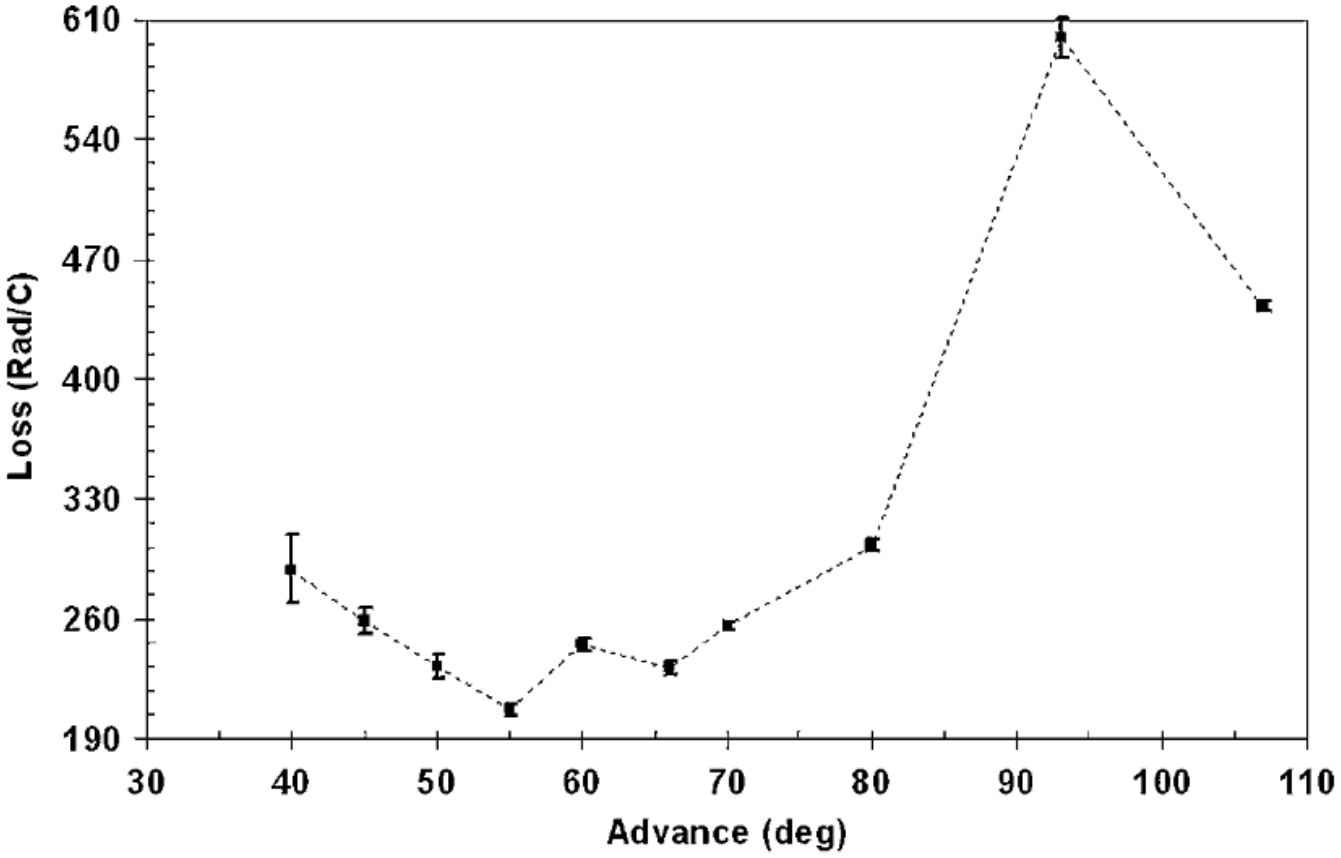

Beam losses in SNS accelerator versus zero-current phase advance (Y. Zhang et al., 2010)

Effect of Lattice Resonance

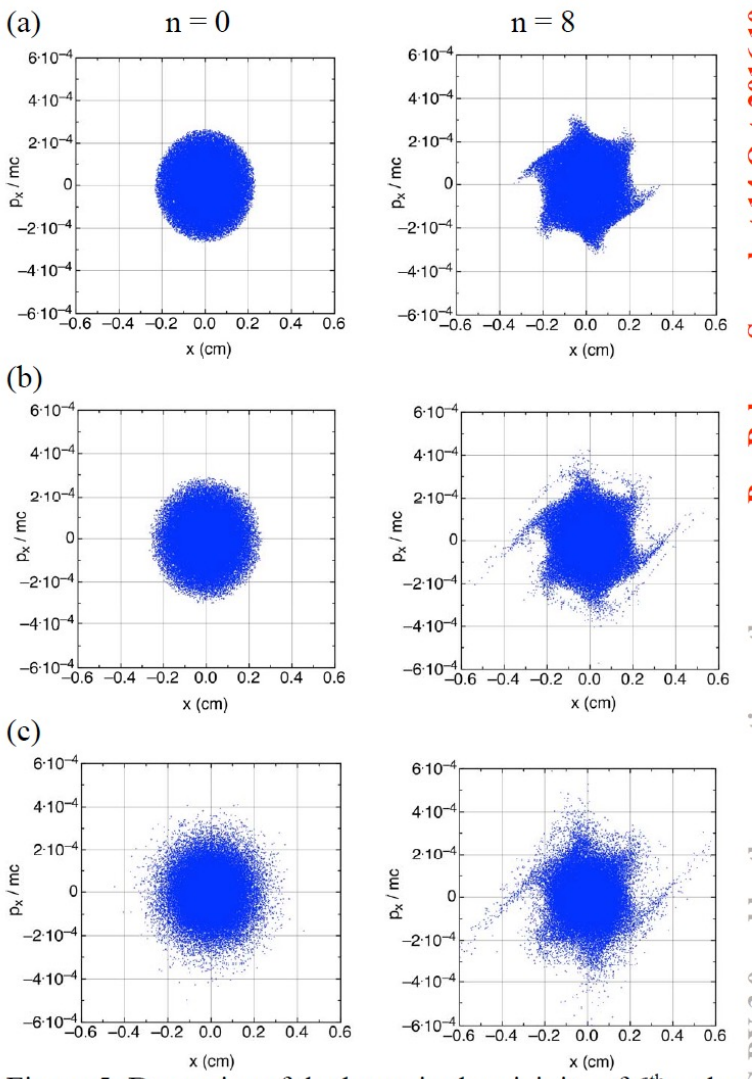

Figure 5: Dynamics of the beam in the vicinity of 6th order resonance for different beam distributions in the lattice with μ_o= 86° : (a) water bag, μ=58° (b) parabolic, μ=54° , (c) Gaussian, μ=38°.

The vector-potential of the magnetic field of a lens with quadrupole symmetry

$$A_z = -[\frac{G_2}{2} r^2 \cos 2\theta + \frac{G_6}{6} r^6 \cos 6\theta + \frac{G_{10}}{10} r^{10} \cos 10\theta + ..]$$

Hamiltonain of averaged particle motion in the vicinity of 6th order resonance:

$$H(J,\psi) = J(\mu_t - \frac{\pi}{3}) + \frac{5}{12}\alpha_6 J^3 + \frac{\alpha_6 J^3}{24}\cos 6\psi$$

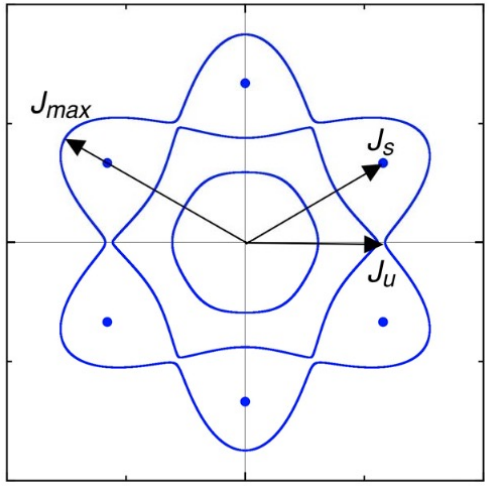

Increase of amplitude of particle trapped into resonance (TUPOB26, NA-PAC 2016)

$$\frac{x_{max}}{x_u} = \sqrt{\frac{J_{max}}{J_u}} = 1.24$$

Excitation of 6th order resonance in quadrupole lattice with phase advance $\mu_o \approx 60^o$

Dark Currents

1. Unchopped beam which comes through chopper due to unsufficient transverse voltage deflecting particles in chopper.

2. Continuous “dark current” of ion source between pulses

3. Beam accelerated during RF turn on/turn off transients.

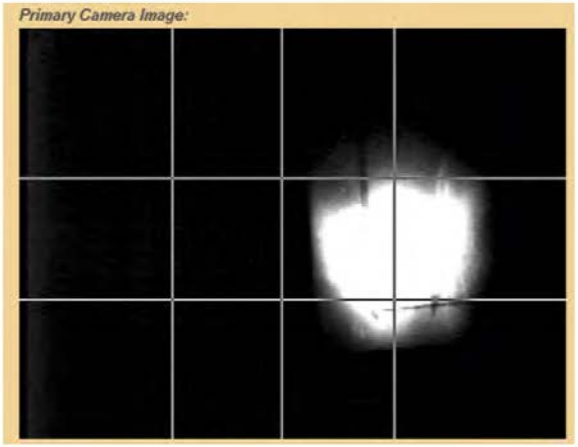

Fig. 15: Example of dark current at a view screen located at the SNS ring injection point. The beam is turned off, yet the dark current is present at levels sufficient to light up the view screen. The phase of the first DTL tank is *not* reversed for this image.

(M.Plum, CERN-2016-002)

Acceleration of H^- Beam

Advantage of H^- beam: multi-turn low-loss beam injection into storage rings and synchrotrons through charge exchange to accumulate large beam charge. Example applications: spallation neutron sources and neutrino production facilities.

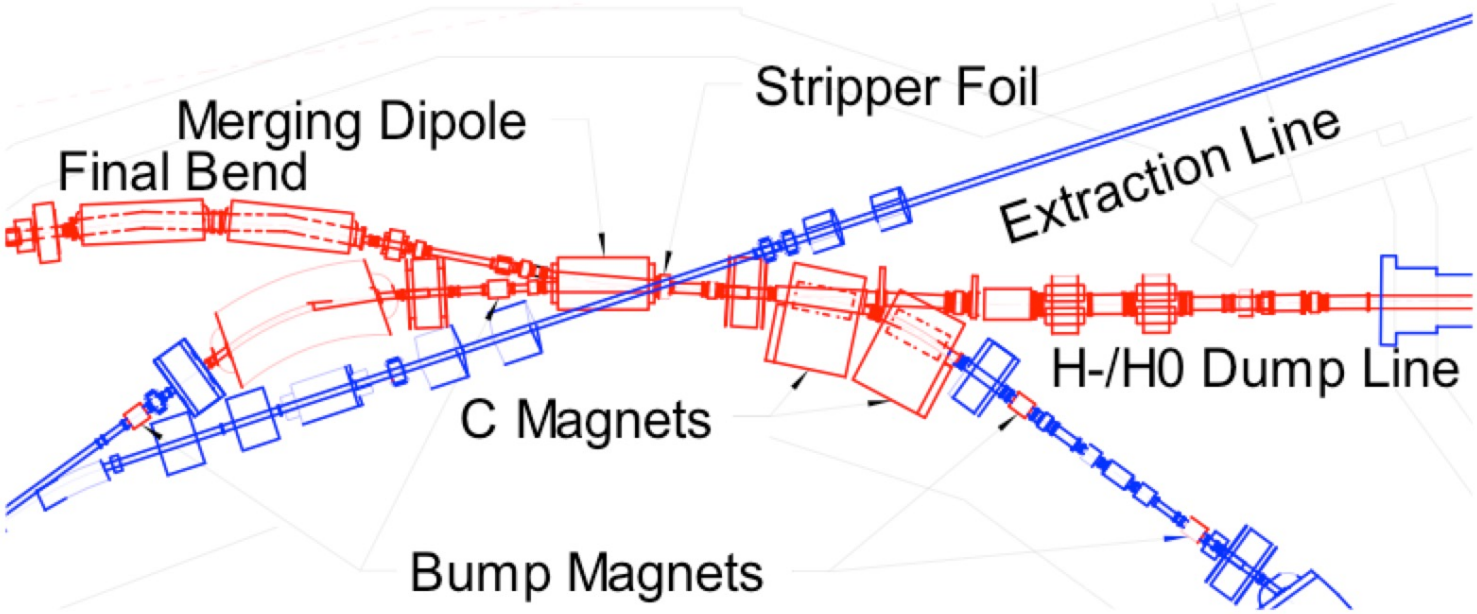

Injection of H^- beam into LANL Proton Storage Ring

H^- Beam Losses in Linac

Beam Loss Mechanisms Observed at Various H^- Linacs (M.Plum, IPAC2013)

Beam loss mechanism	SNS	J-PARC	ISIS	LANSCE
Intra-beam stripping	Yes, dominant loss in SCL linac	Not noted as significant	Not noted as significant	Yes, significant, 75% of loss in CCL
Residual gas stripping	Yes, moderate stripping in CCL and HEBT	Yes, significant, improved by adding pumping to S-DTL and future ACS section	Yes, not significant when vacuum is good, but can be significant if there are vacuum problems	Yes, significant, 25% of loss in CCL
H+ capture and acceleration	Possibly, but not significant concern	Yes, was significant, cured by chicane in MEBT	Not noted as significant	Yes, significant if there is a vacuum leak in the LEBT
Field stripping	Insignificant	Insignificant	Yes, <1% in 70 MeV transport line, some hot spots	Insignificant

H^- Beam Losses in Coupled Cavity Linac (100 MeV-800 MeV)

Energy (MeV)	100	800
Normalized rms beam emitttance (π mm mrad)	0.5	0.7

Beam losses in CCL: 0.1% - 0.2%

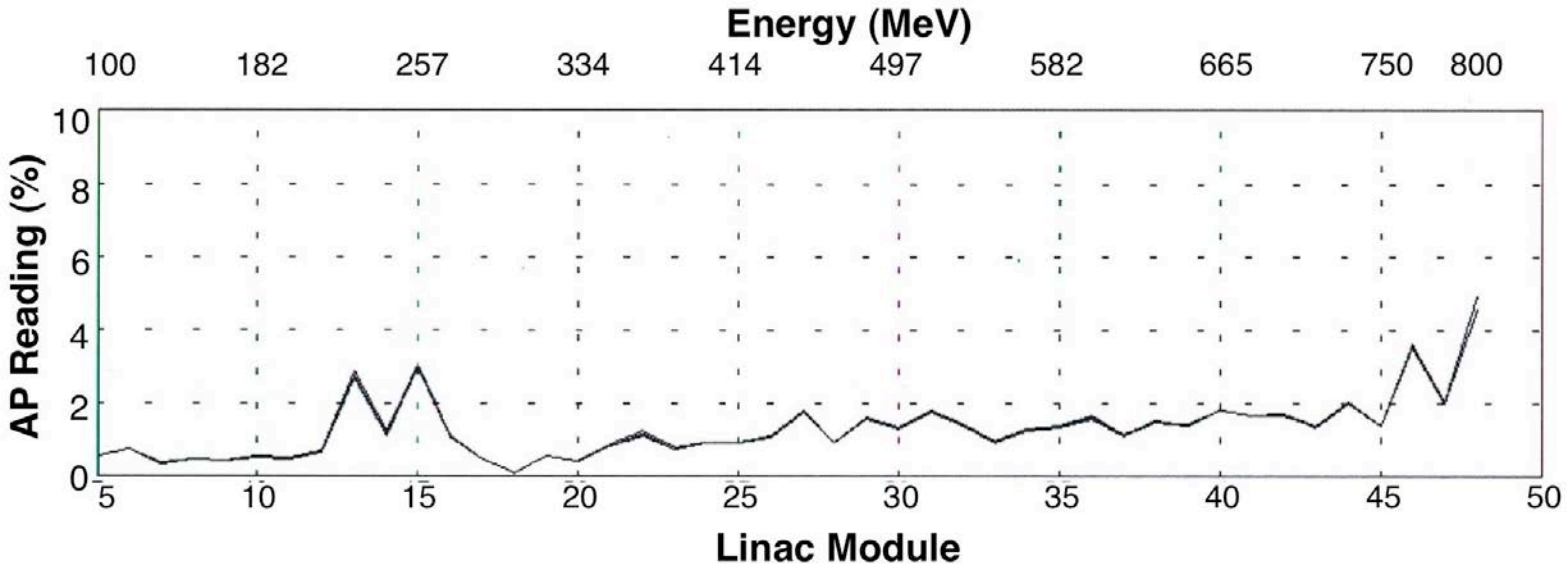

Distribution of H^- beam losses along high-energy part of the linac.

H^- Beam Losses in Coupled Cavity Linac (cont.)

The study performed at LANL indicated significance of Intra Beam Stripping and Residual Gas Stripping on H^- beam losses in Coupled Cavity Linac (L.Rybarcyk, et al, IPAC12, THPPP067):

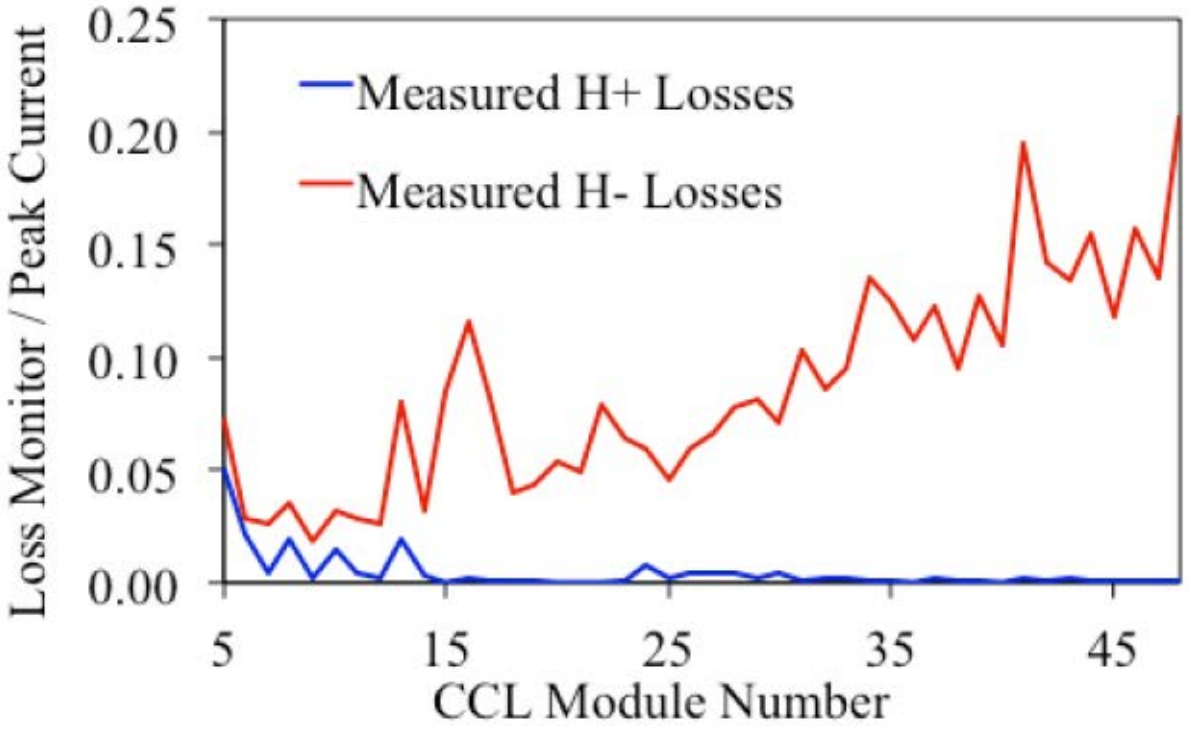

Stripping Mechanism	Beam Fractional Loss
Residual Gas Stripping	2×10^{-4}
Intrabeam Stripping	1.6×10^{-4}
Lorentz Field Stripping	4.5×10^{-11}

Residual Gas Stripping of H^- Beam

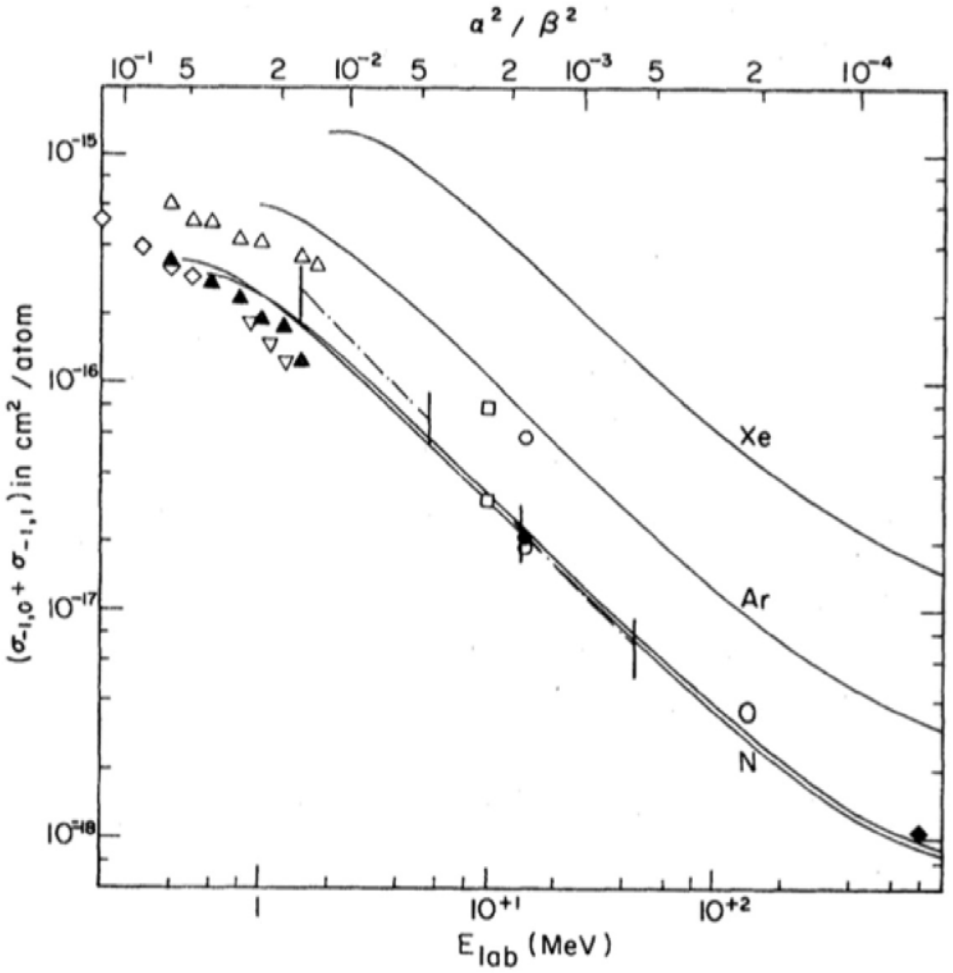

Gas stripping cross-section as a function of H^- beam energy, for various residual gases

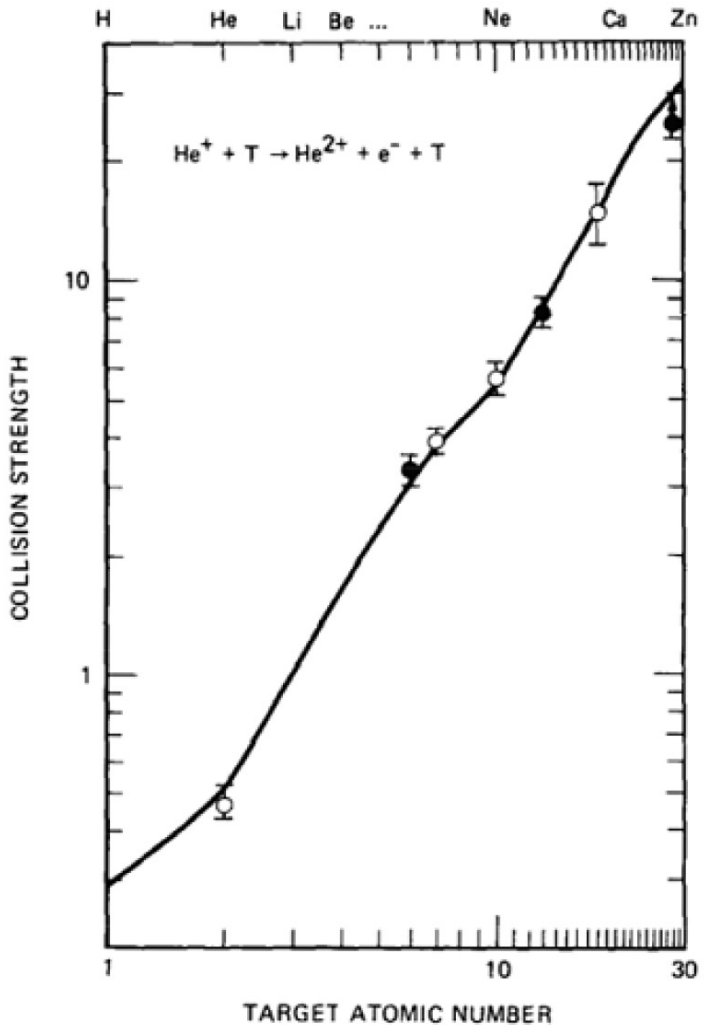

Gas stripping cross-section as a function of atomic number.

Los Alamos NATIONAL LABORATORY

Residual Gas Stripping of H^- Beam (cont.)

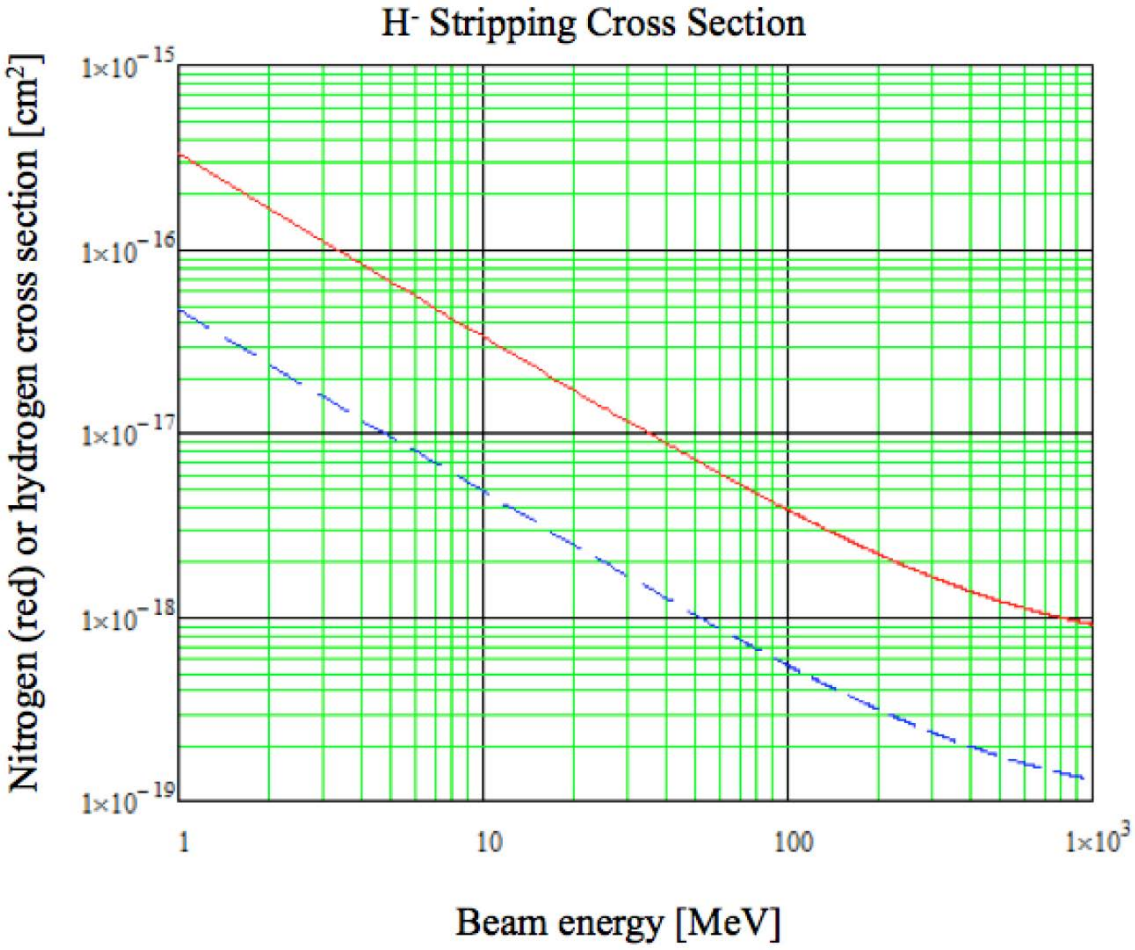

Gas stripping cross-sections for nitrogen or oxygen (solid red line) and hydrogen (blue dashed line) as a function of beam energy.

Residual Gas Stripping of H^- Beam (cont.)

The cross section for double stripping (H^- to H^+) is about 4% of the cross section for single stripping (H^- to H^o).

In a typical accelerator, the residual gases are mainly H_2 , H_2O, CO, CO_2 (low atomic numbers molecules).

With increasing of beam energy, the stripping cross section drops, but beam power increases. With the given gas pressure, residual gas stripping results in increase of beam loss with energy (increase of beam power dominates over dropping cross section).

Allowable gas pressure for acceleration of 1 mA continuous H^- beam current is between 10^{-7} Torr at 100 MeV to 10^{-8} Torr at 1 GeV.

H^+ Capture and Acceleration

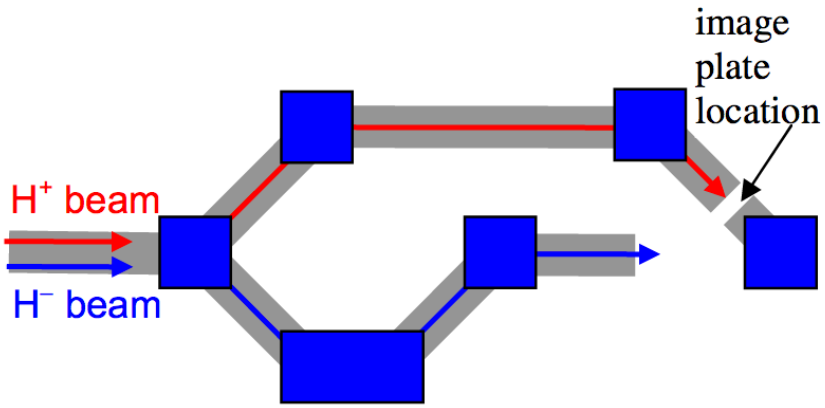

Figure 2: Layout of the beam switchyard showing the location of the image-plate used in detecting the protons that result from stripping of H^- ions. Downstream of this section H^- beam is bent out of the plane of the drawing for delivery to experiment areas.

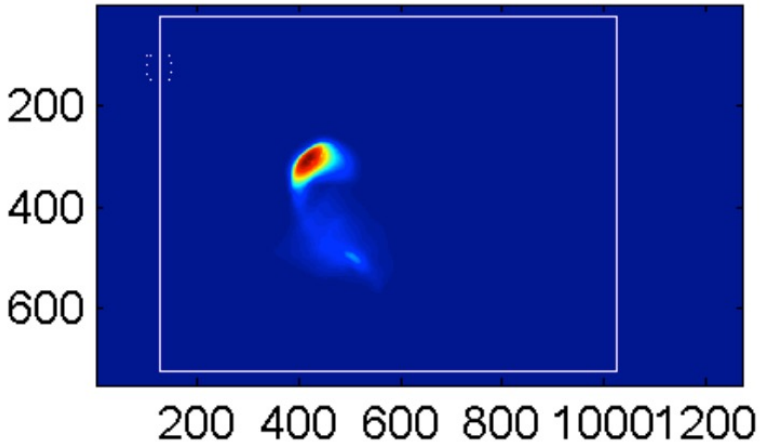

Figure 4: Image plate exposed to the contaminating proton beam with beam plug TRBL01 retracted, i.e. including protons that originate in the LEBT and DTL. The numbers on the axes are pixel numbers. The solid and dashed rectangles indicate the signal and background regions used in the analysis. The color axis has been scaled to show maximum detail in the image.

Detection of H^+ beam after 800 MeV acceleration of H^- beam in LANSCE accelerator (R. McCrady, LINAC 2010).

Magnetic Field Stripping of H^- Ions

Magnetic field is Lorentz transformed into electric field in the rest frame of the H^- beam

$$E[MV/cm] = 0.3\,\beta\gamma\,B[kGs]$$

Life time of H^- ion versus electric field E

$$\tau(E) = \frac{A}{E}\exp\left(\frac{D}{E}\right)$$

$$A = 1.05 \cdot 10^{-14}\ \text{sec}\ MV\,cm^{-1}$$

$$D = 49.25\ MV\,cm^{-1}$$

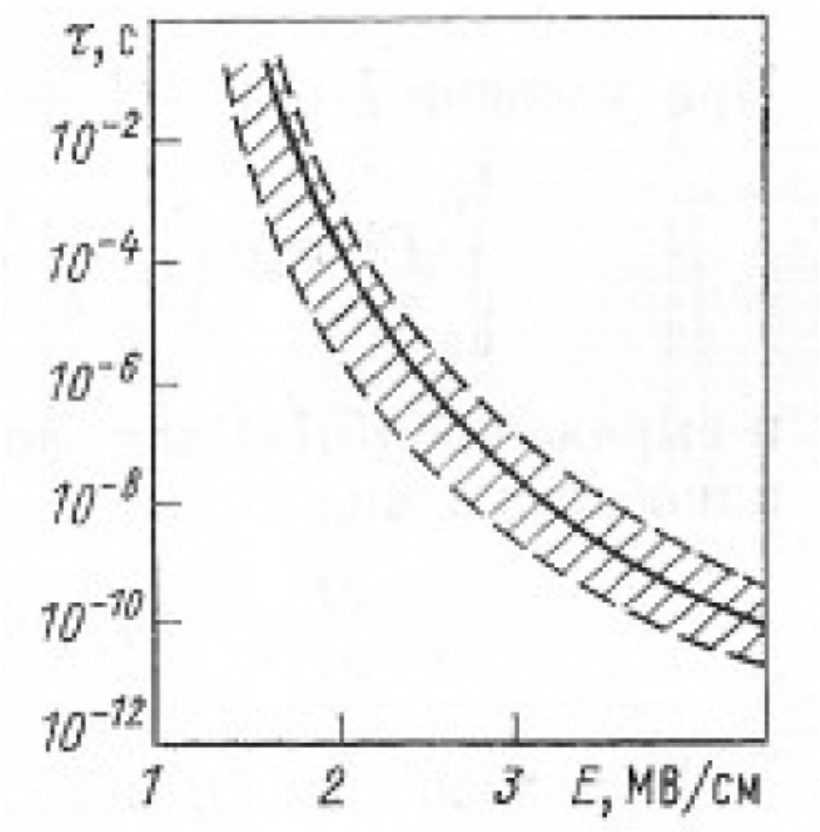

Life time of H^- ion versus electric field

Magnetic Field Stripping of H^- Ions (cont.)

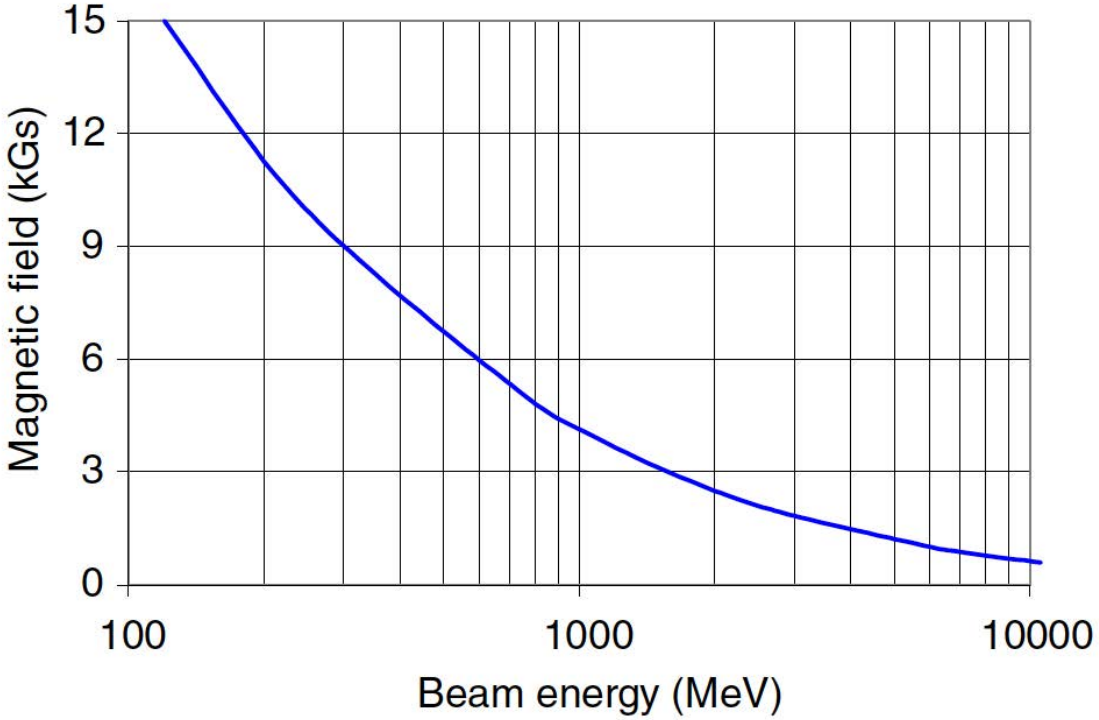

Tolerable magnetic field as a function of beam energy (P.Ostroumov, 2006).

The effect is greatest at high beam energies where the Lorentz transform has the greatest effect. The ISIS facility sees a small amount of field stripping in the 70 MeV transport line between the linac and the ring, at the level of <1%, just enough to create some minor hot spots. SNS, J-PARC and LANSCE have not reported any significant beam loss due to this mechanism (M.Plum, CERN-2016-002).

Intrabeam Stripping in H- Linacs

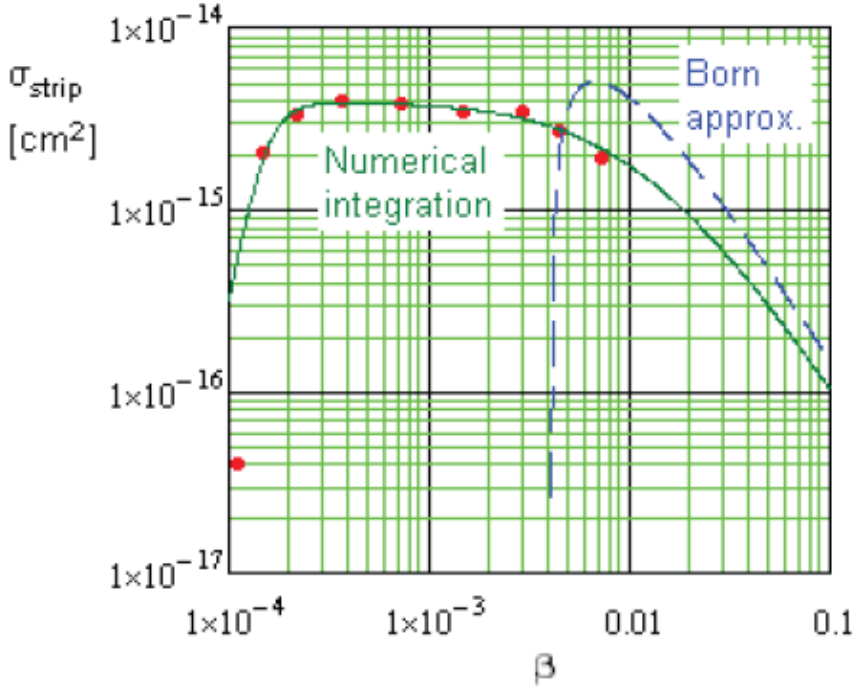

Figure 1: Comparison of Eq. (1) predictions (green solid line) to the numerical simulations of Ref. [5] (red dots), and to the results of Born approximation of Ref. [6] (dashed blue line).

(V.Lebedev et al, LINAC 2010)

Transforming Eq. (4) to the laboratory frame one obtains the relative intensity loss per unit length travelled by the bunch:

$$\frac{1}{N}\frac{dN}{ds} = \frac{N\sigma_{\max}\sqrt{\gamma^2\theta_x^{\,2}+\gamma^2\theta_y^{\,2}+\theta_s^{\,2}}}{8\pi^2\sigma_x\sigma_y\sigma_s\gamma^2}F\left(\gamma\theta_x,\gamma\theta_y,\theta_s\right), \qquad (7)$$

where γ is the relativistic factor, $\sigma_{x,y}=\sqrt{\varepsilon_{x,y}\beta_{x,y}}$ are the transverse rms bunch sizes, $\theta_{x,y}=\sqrt{\varepsilon_{x,y}/\beta_{x,y}}$ are the transverse local rms angular spreads, σ_s and θ_s are the rms bunch length and the relative rms momentum spread.

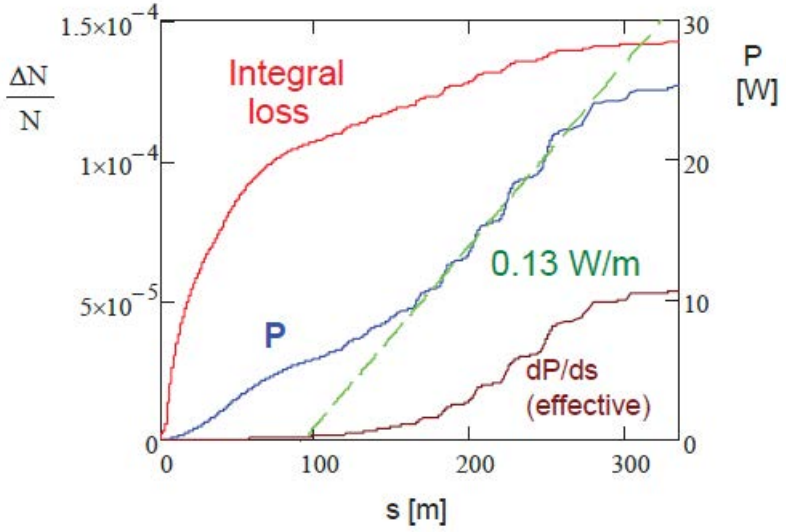

Figure 3: Integrals over linac length for the relative particle loss rate and the power density due to particle loss.

Intrabeam Stripping in H- Linacs (cont.)

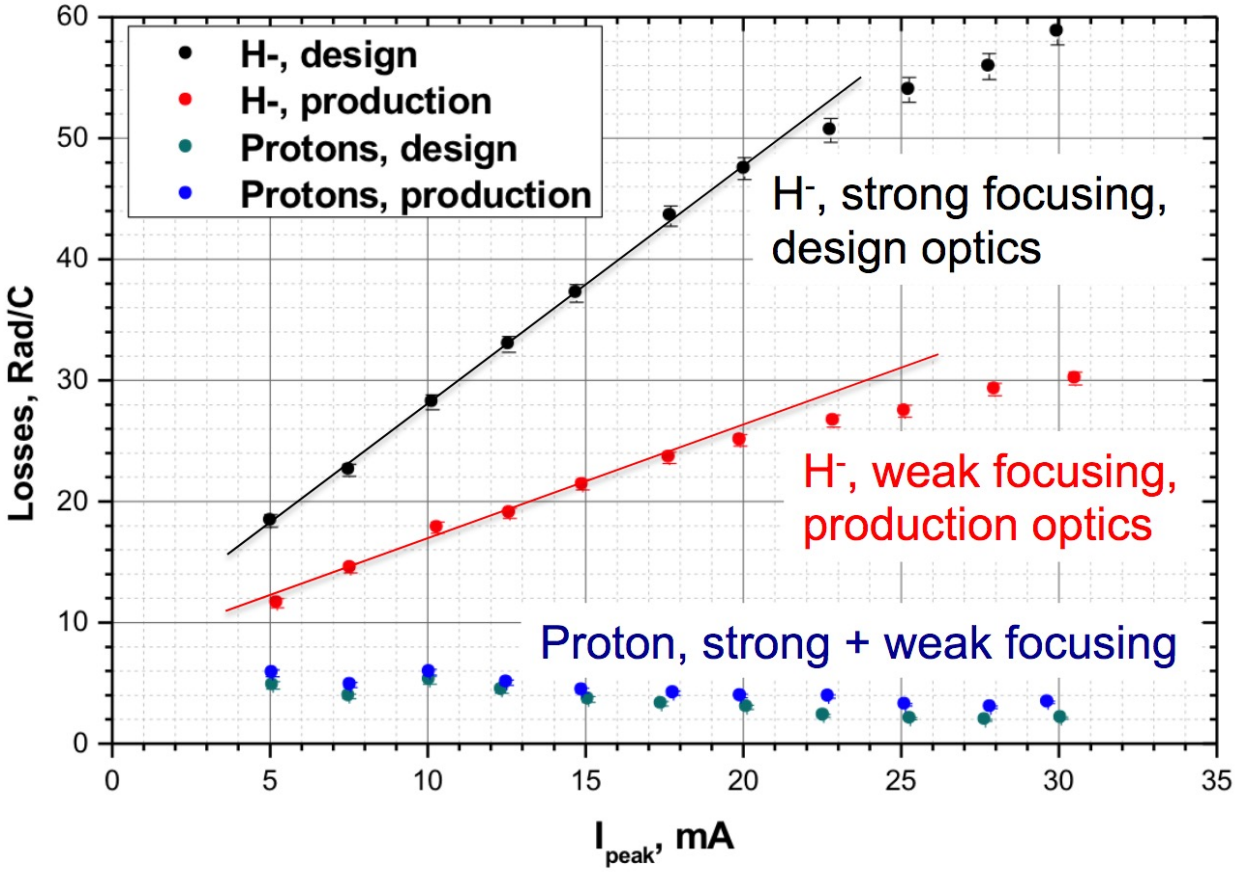

Beam loss versus beam current for protons and H- beams for the design and production optics (A. Shishlo et al, "First Observation of Intrabeam Stripping of Negative Hydrogen in a Superconducting Linear Accelerator," PRL (2012)).

Black Body Radiation

The photodetachment can be produced by black-body radiation of thermal photons emitted from the beam pipes. Such photons can reach sufficient energy in the reference frame of a relativistic beam for H^- stripping.

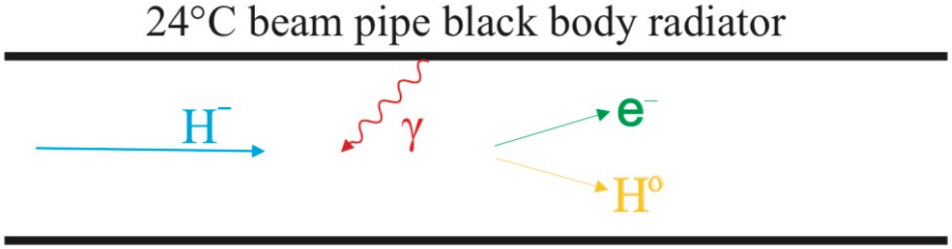

Stripping by black-body radiation of a beampipe (J.-P. Carneiro, 2007).

Figure 10.1. Spectrum of black body radiation

$$f(x)\,dx \propto \frac{x^3}{e^x - 1}\,dx$$

in terms of the dimensionless frequency x.

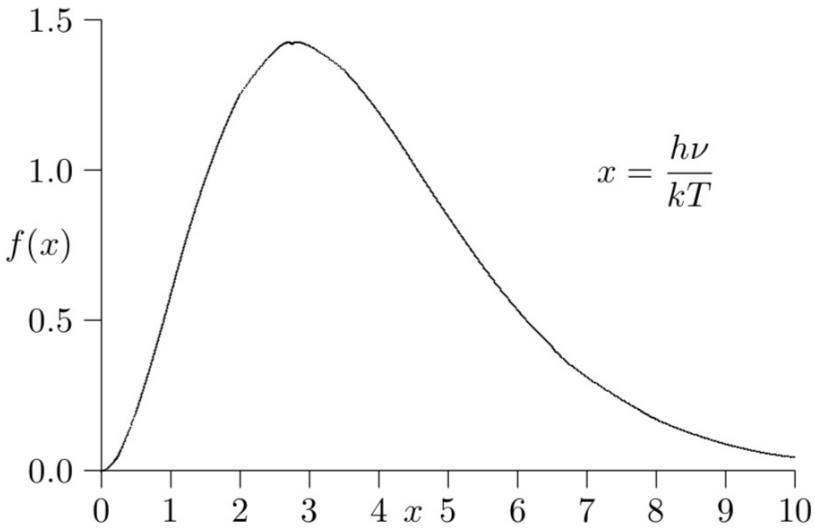

The energy density of thermal photons emitted from beam pipe per unit volume at temperature T within photon frequency interval dv is given by the Planck formula:

$$S_\upsilon(\upsilon,T) = \frac{8\pi h}{c^3}\frac{\upsilon^3}{e^{h\upsilon/k_BT} - 1}$$

where Boltzmann constant: k_B = 8.617333262145 x 10^{-5} eV/K

Plank constant: $h = 6.62607015 \times 10^{-34}$ J·Hz^{-1}

Cross Section of Photodetachment Process

The cross-section of the photodetachment process in the rest frame of H^- beam $\sigma = \sigma(E')$:

$$\sigma(E') = 8\sigma_{BB}^{\max} E_o^{3/2} \frac{(E' - E_o)^{3/2}}{E'^3}$$

where E' is the photon energy in the H^- rest frame;

the maximum black-body stripping cross-section:

$$\sigma_{BB}^{\max} = 4.2 \cdot 10^{-21} m^2$$

E_o = 0.7543 eV is the electron binding energy for H^- ion

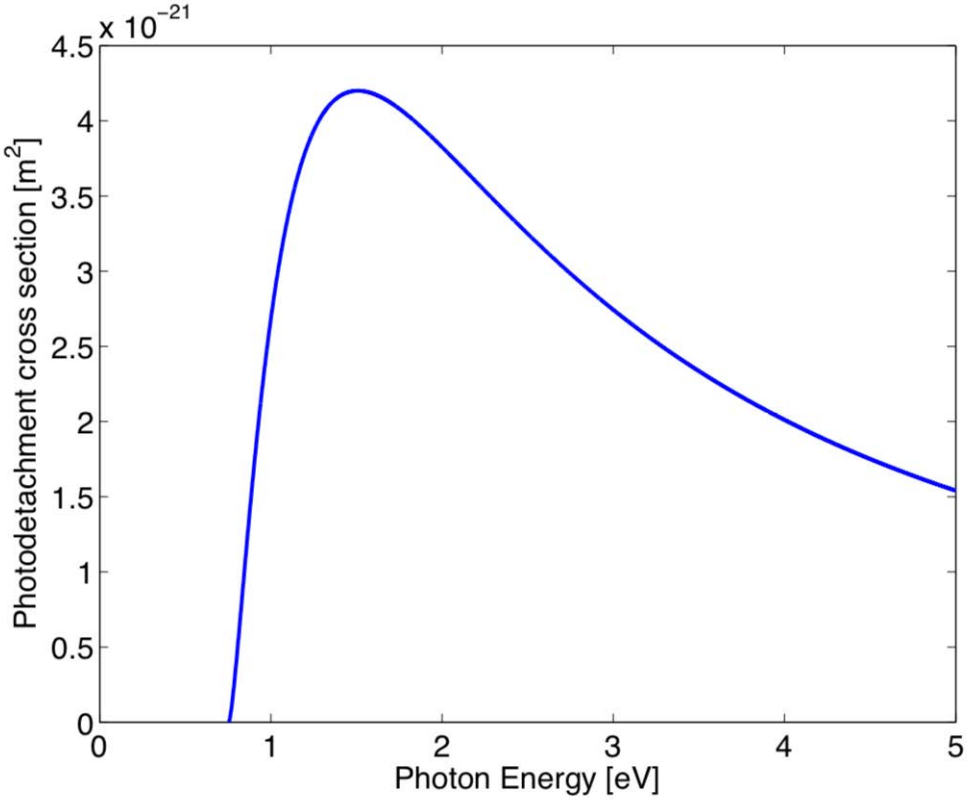

H^- photo-detachment cross-section.

“Lorentz Boost”

Lorentz transformation of the photon energy in laboratory frame E to that in the beam rest frame E' (“Lorenz boost”)

$$E' = \gamma E(1 + \beta \cos\theta)$$

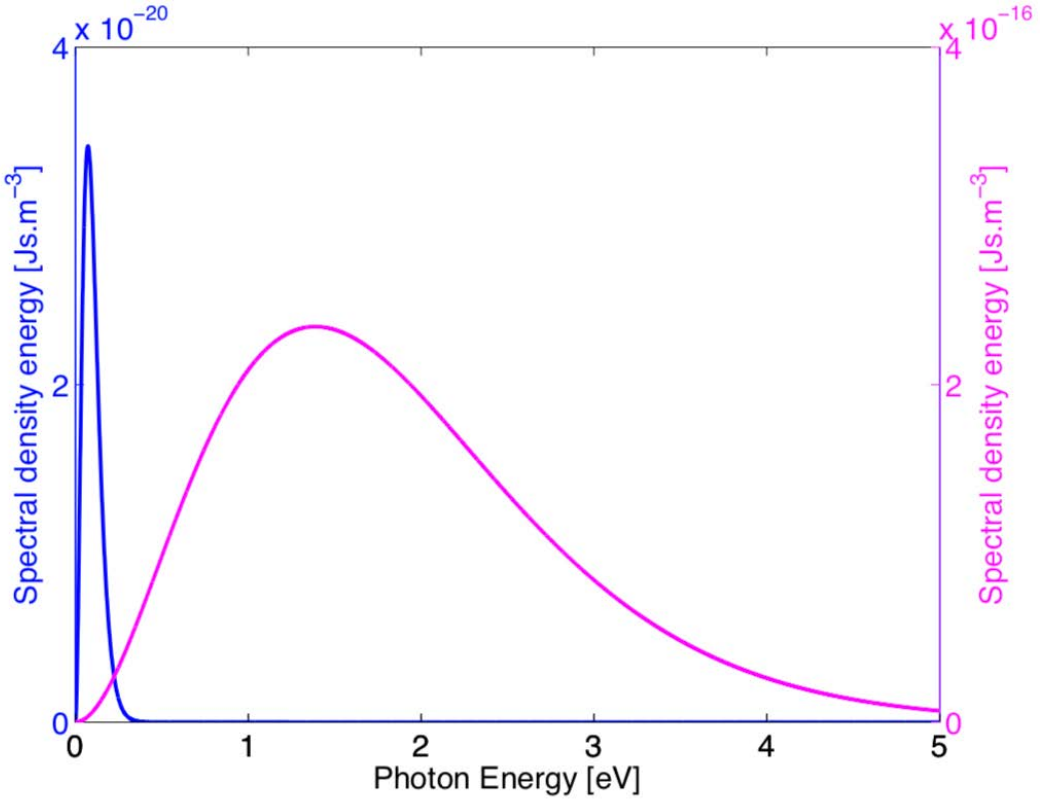

Photons spectral density energy in the laboratory frame (300 K) and Doppler shifted to 8 GeV H^- rest frame . (J.-P. Carneiro, Beams-doc-2740 , 2007).

Beam Loss due to Black Body Radiation

Fraction lost per unit length (H. C. Bryant and G. H. Herling, Journal of Modern Optics, 2006).

$$\frac{\mathrm{d}^3 r}{\mathrm{d}\Omega \mathrm{d}\nu \mathrm{d}l} = \frac{(1+\beta\cos\alpha) n(\nu)\sigma(\nu')}{4\pi\beta}$$

Total loss per unit length:

$$\frac{1}{\mathrm{L}} = \int_0^\infty \mathrm{d}\epsilon \int_0^\pi \mathrm{d}\alpha \frac{\mathrm{d}^3 r}{\mathrm{d}\epsilon \mathrm{d}\alpha \mathrm{d}l}$$

or (J.-P. Carneiro, "H- Stripping Equations and Application to the High Intensity Neutrino Source", FNAL Report Beams-doc-2740, (2007)):

$$\frac{1}{\mathrm{L}} = \frac{8\sigma_{max} E_0^{3/2}}{2\pi^2 \beta\gamma^3 (\hbar c)^3} \int_0^\infty \mathrm{d}E' \int_{-1}^{+1} \mathrm{d}u \cdot \frac{1}{(1+\beta u)^2} \cdot \frac{(E'-E_0)^{3/2}}{E'} \frac{1}{[\exp(E'/kT\gamma(1+\beta u)) - 1]}$$

The loss rate of H^- beam due to black body at temperature T =300K

W =1 GeV 3 x 10^{-9} m^{-1} (negligible)

W = 8 GeV 7.8 x 10^{-7} m^{-1} (significant)

Cooling of the beam pipe at 150 K will reduce losses of 8 GeV beam to the acceptable level of 2.5 x 10^{-8} m^{-1}.

Beam Loss Mitigation

Table 3: Some methods of beam loss mitigation

Cause of beam loss	Mitigation
Beam halo—both transverse and longitudinal	Scraping, collimation, better matching from one lattice to the next, magnet and RF adjustments
Intra-beam stripping	Increase beam size (both transverse and longitudinal)
Residual gas stripping	Improve vacuum
H^+ capture and acceleration	Improve vacuum, add chicane at low energy
Magnetic field stripping	Avoid by design
Dark current from ion source	Deflect at low energy, reverse (phase shift) RF cavity field when beam is turned off
Off-normal beams (sudden, occasional beam losses)	Turn off beam as fast as possible, track down troublesome equipment and modify to trip less often

(M.Plum, CERN-2016-002)